Static and Dynamic Moments for any Plane within a Straight Solid Slab Bridge Caused by the Crossing of a Truck

Omar Mohammed [1,3] *, Arturo González [2,3]

[1] Researcher, email: omar.sattar@ucdconnect.ie

[2] Associate Professor, email: arturo.gonzalez@ucd.ie

[3] School of Civil Engineering, University College Dublin, Ireland

* Corresponding author. Postal address: School of Civil Engineering, University College Dublin, Newstead, Belfield, Dublin 4, Ireland.

Phone number: +353 1 7163229.

Email address: omar.sattar@ucdconnect.ie, omaralanni1984@gmail.com

Abstract

A lot of research has been carried out to explain the manner in which longitudinal moments of a bridge respond to traffic. The total longitudinal bending moment is made of 'static' and 'dynamic' components, which vary with time as a result of the inertial forces of the bridge and changes in value and point of application of the forces of the vehicle. However, there is limited evidence about how bending moments at planes other than longitudinal, or twisting moments, act in response to a moving vehicle. For the first time in the literature, this paper analyses the total resultant moments ('static' + 'dynamic') for any plane orientation (from 0 to 360°) at any location of a solid slab deck due to the crossing of a vehicle. The bridge is modelled as a simply supported straight orthotropic plate and the vehicle is modelled as a three-dimensional 5-axle articulated system composed of interconnected sprung and unsprung masses. Simulations are performed for three vehicle transverse paths and three speeds. Using Wood and Armer equations, the resultant moment at any plane orientation can be obtained from equilibrium of bending and twisting moments acting on longitudinal and transverse planes. Maximum twisting

moments develop in planes at 45° with longitudinal and transverse planes. Bending moments reach maximum and minimum values at longitudinal and transverse planes. Nevertheless, the moments acting on other plane orientations cannot be ignored in order to accurately assess whether the moment capacity of the bridge provides adequate safety. Therefore, the amount of slab reinforcement will be sufficient provided that the moment capacity exceeds the applied moment for any location and plane. Critical locations with highest values of sagging, hogging and twisting are identified in the bridge, and the dynamic amplification associated to the applied moments is evaluated. Bridge codes such as the Eurocode employ a unique built-in dynamic amplification factor for moment that depends only on the bridge length and the number of lanes. This paper shows how to perform an improved assessment allowing for changes in dynamic behaviour with location and plane orientation, which may prevent needless expense in bridge rehabilitation.

Key words: Vehicle Bridge Interaction; Bridge slab; Dynamic Amplification Factor; Moments; Traffic loading; Bridge dynamics

1. Introduction:

Solid slab deck sections are commonly found in short span bridges, spanning to about 21 m [1,2]. These are made of in-situ or a mix of precast inverted T-beams and in-situ concrete [3]. For medium-span bridges, there is a substantial increase in the self-weight of the solid slab and the challenges of construction; hence, beam-and-slab decks are generally preferred. The thickness of the solid slab deck is significantly smaller than the width and length. Solid slab decks carry out vertical loads to the supports by a combination of moments and shear forces. Thin plate theory is commonly accepted for modelling the bending behaviour of these decks. The deck is assumed to be uncompressible and the deflection of the plate is attributed to

bending alone (i.e., shear distortion makes no substantial contribution to deflection). These assumptions are a simplification of the true behaviour, but are justified by the fact that the performance of these bridge slabs, being relatively thin, is dominated by bending rather than shear deformation [5]. Figure 1 shows the total moments acting about mid-depth of a plate element with longitudinal dimension 'a' and transverse dimension 'b'.

The bending capacity of the slab must be sufficient to withstand not only the maximum bending moments at longitudinal and transverse planes, but any moment regardless of the plane. For that purpose, the total moments, M_x and M_y, acting in longitudinal and transverse planes respectively, can be considered as vectors and combined to attain the resultant moment for a plane at any specific angle from imposing equilibrium. Here, it is worth to mention the role played by Wood and Armer in slab design, who suggest an expression to determine the bending moment capacity per unit breadth in longitudinal and transverse directions (orthogonal reinforcement) necessary to withstand the maximum applied bending moment irrespective of plane orientation [4]. The notation m_x (= M_x / b) refers to bending moment per unit breadth acting on a plane of normal the longitudinal direction x (i.e., perpendicular to the boundary delimited by the bridge supports). Similarly, the transverse bending and twisting moments per unit breadth are represented by the symbols m_y (= M_y / a) and m_{xy} (= M_{xy} / b) respectively. Therefore, m_{xy} is equal to m_{yx} due to equilibrium. There are numerical and experimental investigations on how these perpendicular moments affect the static response of a concrete slab [5-9]. Longitudinal stresses σ_x due to m_x, are found to be larger than transverse stresses σ_y, due to m_y, with first cracks developing at 45°. As the span of the slab gets longer, it is evident that the static longitudinal bending becomes more dominant. In the case of a concrete slab bridge traversed by a vehicle, there will be a 'dynamic' component in addition to the 'static' component [10]. Bakht and Pinjarkar [11], Inbanathan and Wieland [12] and Wang and Deng [13] quantify this 'dynamic' component with a term named dynamic Impact Factor (IM), which

takes into account the maximum of the two responses ('dynamic' and 'static'). Dynamic Load Allowance (DLA) [14–16] and Dynamic Amplification Factor (DAF) [17–19] are other popular definitions to characterize the 'dynamic' component. DAF is defined as the ratio of maximum total ('static' plus 'dynamic' components) response to the maximum 'static' response at a specific bridge location. Cantero et al. [20] put forward a new definition, i.e., Full Dynamic Amplification Factor (FDAF), to cover for the fact that the selected bridge location may not hold the worst possible scenario. FDAF is given by the ratio of the maximum total response taking into account all bridge sections to the maximum 'static' response at a particular section taken as reference (typically mid-span). By definition, FDAF is always equal or greater than DAF for a given section. A considerable amount of information is provided by earlier authors on DAF or equivalent terms due to a moving load. However, most of existing literature investigate deflections or the longitudinal bending moment/strains (i.e., m_x), and only a few publications have examined DAF associated to other load effects (i.e., DAF of shear by [21]). Therefore, there is a need in the literature to address the dynamic impact experienced by moments in planes other than longitudinal as a result of the moving traffic. Without this information, it is not possible to gather an accurate picture of the true moment capacity needed to ensure the safety of a slab. For this purpose, Section 2 describes the mathematical models that will be employed to calculate the response of the bridge to a moving vehicle. The slab deck is modelled using thin plate Finite Element (FE) theory and the truck is represented by a 5-axle tractor and semitrailer configuration. Section 3 calculates bending and twisting moments acting on longitudinal and transverse planes for a 9m long bridge, three transverse vehicle paths (travelling centred over the bridge centreline and at other two eccentricities) and three vehicle speeds (15, 20 and 25 m/s). Section 4 calculates moments ('static' and total) for any plane orientation θ, where θ is the angle that the normal to the plane makes with the x-direction (i.e., $\theta = 0$ is the longitudinal plane where m_x is acting, and $\theta = 90$ is the transverse plane where m_y

is acting). Finally, the critical locations holding the largest moments are discussed and Section 6 provides conclusions.

2. Simulations Models

2.1. Bridge Model

A simply supported solid slab deck of 9 m width and 9 m span length is considered. The bridge is modelled as an orthotropic thin plate discretized using the FE method into a mesh made of 0.5 m × 0.5 m plate elements. The standard Kirchoff plate element [22,23] contains four nodes and three Degrees Of Freedom (DOFs) per node: the vertical displacement and the rotations about the *x* and *y* axes. This discretization of the displacement field results in a third-order polynomial containing 12 terms. Zienkiewicz [22] and Reddy [23] explain in detail why such a discretization can lead to a discontinuity of the slope across inter-element boundaries. One solution to the problem of the non-conforming plate element is to impose continuity conditions as an additional DOF, such that the fourth DOF at each node is the second derivative of *w* with respect to *x* and *y*. This fourth DOF is also known as nodal twist. Bogner et al [24] first proposed this method for isotropic plates, where the interpolation functions for the DOFs were defined as the products of the Hermite shape functions for an Euler-Bernoulli beam. The full derivation of the 16 DOF orthotropic C_1 plate element employed in this paper can be found in Rowley [25]. Vertical displacements are prevented at each node of end sections above supports. In total, the bridge has 1444 DOFs. The properties of the bridge are presented in Table 1 based on [26,27].

Table 1. Properties of bridge model

Length	9 m
Breadth	9 m
Depth	0.45 m
Modulus of elasticity in longitudinal direction	35×10^9 N/m^2
Modulus of elasticity in transverse direction	32.2×10^9 N/m^2
Shear modulus	14×10^9 N/m^2
Plate density	2500 kg/m^3
Damping ratio %	3
First natural frequency	9.50 Hz

The response of a bridge to time-varying forces can be modelled using Equation (1).

$$M_b\ddot{w}_b + C_b\dot{w}_b + K_b w_b = f_b \quad (1)$$

where M_b, C_b and K_b are the mass, damping, and stiffness matrices respectively of the plate model, and $\ddot{w}_b$, $\dot{w}_b$ and w_b are vectors containing nodal accelerations, velocities and displacements. f_b is the vector of external forces applied to the DOFs of the bridge. Damping is assumed to be Rayleigh type as follows:

$$C_b = \alpha M_b + \beta K_b \quad (2)$$

where α and β are constants defined by $\alpha = 2\zeta\omega_1\omega_2/(\omega_1 + \omega_2)$ and $\beta = 2\zeta/(\omega_1 + \omega_2)$. Here, ω_1 and ω_2 represent the first two natural frequencies of the bridge. Damping ratio ζ is adopted to be 0.03 and the same for all modes [28]. The first natural frequency of the bridge is 9.50 Hz.

2.2. Vehicle Model

The vehicle model is based on a typical 5-axle articulated truck. Two significant bodies can be distinguished, tractor and semi-trailer, which are represented by lumped body masses, m_s and m_T (Figure 2). Each of the axles is modelled as a rigid bar with lumped masses that represent the total mass of the wheel and suspension assemblies. The body masses are linked to lumped axle masses via spring-dashpot systems simulating the suspension. Spring-dashpot systems that

resemble the tyres are used to connect the axle masses to the road surface. In total, the model has 15 DOFs. Tables 2 and 3 provide the geometry and the mechanical properties of the vehicle respectively, based on the work by [20,29].

Table 2. Vehicle geometry

Dimensions: m	
b_1	0.5
b_2	2.5
b_{31}	1.3
b_{32}	2.4
b_{33}	3.5
b_4	4.15
b_5	2.15
a_1	-0.13
a_2	1.10

Table 3. Vehicle properties (subscripts R and L refer to Right and left axle respectively)

Mass and inertia data	
Tractor sprung mass, m_T: kg	4500
Tractor front axle: kg	700
Tractor rear axle: kg	1000
Semitrailer axles: kg	800
Tractor pitch moment of inertia $I_{T\ pitch}$ kg m^2 (about Y-axis)	4875
Tractor rolling moment of inertia $I_{T\ roll}$ (about X-axis)	3000
Semi-trailer sprung mass, m_s: kg	31450
Semi-trailer pitch moment of inertia $I_{s\ pitch}$ kg m^2 (about Y-axis)	123000
Semi-trailer rolling moment of inertia $I_{s\ roll}$ (about X-axis)	21000
Spring rates: kN/m (suspensions)	
K_{1R}, K_{1L}	200
K_{2R}, K_{2L}	500
$K_{3\text{-}5R}$, $K_{3\text{-}5L}$	375
Spring rates: kN/m (tyre)	
K_{t1R}, K_{t1L}	875
K_{t2R}, K_{t2L}	1750
$K_{t3\text{-}5R}$, $K_{t3\text{-}5L}$	1750
Viscous damping rates: kNs/m (suspensions)	
$C_{1\text{-}5R}$, $C_{1\text{-}5L}$	5
Viscous damping rates: kNs/m (Tyre)	
$C_{t1\text{-}5R}$, $C_{t1\text{-}5L}$	3

The range of pitching and rolling body frequencies falls within 1.5 Hz to 4.5 Hz and the hopping axle frequencies go from 9 Hz to 16 Hz (Table 4), in agreement with values published by [30].

Table 4. 5-axle vehicle frequencies in Hz

symbol	property	value
f_{v1}	Tractor bounce	1.48
f_{v2}	Tractor pitch	2.3
f_{v3}	Tractor roll	3.0
f_{v4}	Semitrailer pitch	1.49
f_{v5}	Semitrailer roll	1.58
f_{v6}	1st axle hop left wheel	8.9
f_{v7}	1st axle hop right wheel	8.9
f_{v8}	2nd axle hop left wheel	10.7
f_{v9}	2nd axle hop right wheel	10.7
f_{v10}	3rd axle hop left wheel	11.6
f_{v11}	3rd axle hop right wheel	11.6
f_{v12}	4th axle hop left wheel	11.6
f_{v13}	4th axle hop right wheel	11.6
f_{v14}	5th axle hop left wheel	11.6
f_{v15}	5th axle hop right wheel	11.6

The static gross vehicle weight is distributed amongst axles 1 to 5 based on the percentages given by [31]: 12.70 % (front axle), 27.70 % (2nd axle) and 19.87 % (any of the axles in the rear tridem). Static wheel weights are given in Table 5.

Table 5. Static wheel weights (kN) (subscripts R and L refer to right and left axle respectively)

$P_{1R,}$ P_{1L}	24.93
P_{2R}, P_{2L}	54.39
P_{3R}, P_{3L}	38.99
P_{4R}, P_{4L}	39.01
P_{5R}, P_{5L}	39.01

The equations of motion of a vehicle model can be obtained imposing equilibrium of all forces and moments that act on the masses. The terms in these equations can be ordered according to the DOFs and placed in matrix form as follows:

$$M_v\ddot{w}_v + C_v\dot{w}_v + K_v w_v = f_v \quad (3)$$

where M_v, C_v and K_v are mass, damping and stiffness matrices of the vehicle respectively, and $\ddot{w}_v$, $\dot{w}_v$ and w_v are the vectors corresponding to nodal accelerations, nodal velocities and nodal displacements. f_v is a vector containing the time-varying forces imposed on the vehicle's DOFs. This model assumes negligible lateral and yaw movement.

2.3. Road Profile

The roughness of the road surface is a major cause of dynamic excitation in vehicle-induced bridge vibrations [32–36]. An artificial road profile can be generated using the Power Spectral Density (PSD) of vertical irregularities along with the inverse fast Fourier transform technique explained by [37]. For each spatial wave frequency, a random phase angle $\emptyset_i$ is sampled from a uniform probabilistic distribution in the range 0-2π. An 'A' class road carpet, i.e. 'very good' according to the International Organization for Standardization (ISO 1995)[38], is produced using a geometric spatial mean of 16×10^{-6} m3/cycle [39]. Finally, a moving average filter is applied to the road irregularities across a distance of 0.24 m to simulate the tyre contact patch [40,41]. Figure 3 shows the resulting class 'A' carpet used for the surface of the bridge. This bridge surface is preceded by a 100 m approach generated using the same procedure. The purpose of the road approach is to induce vibrations in the vehicle prior to entering the bridge that will simulate initial conditions of dynamic equilibrium.

2.4. Uncoupled VBI Algorithm

An uncoupled Vehicle-Bridge Interaction (VBI) algorithm is employed for calculating the response of the plate model to the crossing of the 5-axle truck at uniform speed. The equations of motion of the vehicle (Equation (3)) and the bridge (Equation (1)) are treated as two separate subsystems. These equations are solved via application of the Newmark-Beta direct integration method with a time increment of 0.002 s and values for the integration constants of delta = 0.5 and beta = 0.25. An iterative process is carried out at each time step as follows. Initially, forces acting on the DOFs of the vehicle (f_v) are calculated using Equation (3) based on the road profile 'only'. The wheel forces defined by f_v need to be converted to equivalent forces acting on the bridge nodes (f_b) before calculating the bridge response. Equation (4) is used to distribute each wheel force from its point of application to the nodes of the plate element directly underneath.

$$f_b = L \times f_v \tag{4}$$

where f_b is a matrix p x 1, f_v is a vector p_f x 1, and L is an $p \times p_f$ location matrix that relates the p_f wheel forces to equivalent forces acting on the p DOFs of the bridge. Each column of the location matrix L maps one of the p_f forces to the DOFs associated with the particular underlying element as a product of the numerical value of the shape functions for that point in time. In this way, the time-varying location matrix L becomes a function of the shape functions of a 2D plate element as follows:

$$L=\begin{bmatrix} 0 & 0 & ... & 0 & ... & 0 \\ . & . & ... & . & ... & . \\ N_1(x_1,y_1) & . & ... & . & ... & . \\ N_2(x_1,y_1) & N_1(x_2,y_2) & ... & . & ... & . \\ . & N_2(x_2,y_2) & ... & N_1(x_i,y_i) & ... & . \\ N_{16}(x_1,y_1) & . & ... & N_2(x_i,y_i) & ... & N_1(x_{10},y_{10}) \\ . & N_{16}(x_2,y_2) & ... & . & ... & N_2(x_{10},y_{10}) \\ . & . & ... & N_{16}(x_i,y_i) & ... & . \\ . & . & ... & . & ... & N_{16}(x_{10},y_{10}) \\ . & . & ... & . & ... & . \\ 0 & 0 & ... & 0 & 0 & 0 \end{bmatrix} \quad (5)$$

where $N_1(x_i, y_i)$ to $N_{16}(x_i, y_i)$ are the shape functions corresponding to the 16 DOFs of the plate element. Here, column i represents the distribution of the wheel force i to the DOFs of the element that the force is acting on, and x_i and y_i are the time-varying longitudinal and transverse distances from the wheel force i to a node of the element. I.e., columns 1, 2, 3 … and 10 distribute the first, second, third … and tenth wheel forces of the vehicle respectively to the DOFs of the bridge. The four shape functions corresponding to the vertical displacement, the rotations about the x- and y- directions and the twist of one node of the plate element are given by Equations (6), (7), (8) and (9) respectively.

$$N_1(x_i,y_i)=(b+2y_i)(b-y_i)^2(a+2x_i)(-x_i+a)\frac{1}{a^3b^3} \quad (6)$$

$$N_2(x_i,y_i)=-y_i(b-y_i)^2(a+2x_i)(-x_i+a)^2\frac{1}{a^3b^2} \quad (7)$$

$$\begin{aligned} N_3(x_i,y_i)&=x_i(b-y_i)(-2x_iab^3+x_i^2b^3+a^2b^2-2x_iy_iab^2+x_i^2y_ib^2 \\ &+y_ia^2b^2-14x_iy_i^2ab+10x_i^2y_i^2b-2y_i^2a^2b+18x_iy_i^2a^2-12x_i^2y_i^2a)\frac{1}{a^2b^4} \end{aligned} \quad (8)$$

$$\begin{aligned} N_4(x_i,y_i)&=x_iy_i(b-y)(-2x_iab^2+x_i^2b^2+a^2b^2-7x_iy_iab \\ &+5x_i^2y_ib-y_ia^2b+9x_iy_ia^2-6x_i^2y_ia)\frac{1}{a^2b^3} \end{aligned} \quad (9)$$

where a and b are the dimensions of the plate element.

The vector f_b is then employed in Equation (1) to calculate bridge displacements (w_b), which are subsequently employed together with the road profile to recalculate the vehicle forces f_v in a 2nd iteration, and so on. The stopping criterion employed here is based on [42], who specify that the variation between the bridge deflections, w_b, of two consecutive iterations must be less than 2% of the highest bridge deflection. Once the criterion is achieved, the forces of the vehicle are positioned at new coordinates on the bridge and the iterative process is carried out again. Cantero et al. [2, 29, 43] provide further details on this uncoupled algorithm. The latter is coded with the help of MATLAB because of the flexibility it offers. The program has been validated against alternative VBI approaches and experimental data [30]. The simulations are carried out using a computer with 32 GB RAM memory, i7-3770 core processor and CPU @ 3.4 Hz running MATLAB 2014 on a Windows 7 platform. The computational time to obtain the responses at all FE nodes for one crossing of the vehicle is less than one minute.

Figure 4 depicts the three transverse positions that are considered for the path of the vehicle. There is an equal distance between the centre of gravity of the vehicle's body mass and the outer and inner wheels (Figure 2(b)). The paths of this centre of gravity are at a distance of 0 m (path '2'), 1.5 m (path '1') and 3 m (path '3') from the bridge longitudinal centreline. If the bridge had two traffic lanes situated symmetrically with respect to the bridge centreline, path '1' would approximately correspond to the vehicle travelling in the middle of the lane, path '2' to the vehicle travelling in the middle of the bridge, and path '3' to a rare situation where the vehicle is travelling partially on the shoulder. The distribution of moments in the slab are calculated for nine vehicle scenarios covering these three transverse paths and three speeds: 15, 20 and 25 m/s.

3. Moments in Longitudinal and Transverse Planes

The total ('static' + 'dynamic') values of the FE DOFs are calculated using the procedure described in Section 2.4. m_x, m_y and m_{xy} are then determined for each node of the bridge FE based on the shape functions and constitutive equations of the plate element [22]. 'Static' displacements and rotations can be obtained using Equation (1) for every position of the truck, assuming vehicle axle forces equal to static axle weights and null acceleration and velocity vectors.

Figure 5 illustrates the longitudinal bending moment per unit breadth (m_x) in kN·m/m at the mid-span section, when the vehicle is moving at 20 m/s over path '2' (i.e., centred on the bridge). The variation of total and 'static' m_x with the position of the 1st axle of the truck on the bridge are shown in Figures 5(a) and 5(b) for the node at 3.5 m from the bridge's left edge and for the node at the right edge respectively. It can be seen that the total bending moment oscillates about its 'static' component and that total and 'static' moments reach a maximum value for the same truck location, i.e., first axle at 13.7 m from the 1st support of the bridge. The maximum 'static' and total values are plotted in Figure 5(c) for all FE nodes across the mid-span section. Two peaks of moments can be observed to take place under the paths of the wheels, i.e., at 3.5 m and 5.5 m from the bridge edge. The ratio of total to 'static' moment is relatively larger at the edges than at the centre of the section. As a result, DAF of m_x for the mid-span node at 3.5 m from the edge is equal to 61.92/60.08 = 1.03, and DAF of m_x for the node at the right edge is equal to 43.85/40.77 = 1.07.

The maximum 'static' and maximum total values of m_x shown in Figure 5(c) for the mid-span nodes due to the vehicle travelling along path '2', are obtained for the remaining bridge nodes and the other two vehicle paths, together with the values of m_{xy} and m_y. Figures 6 to 8 provide contour plots for these moments at every node for the three paths of the vehicle travelling at 20

m/s. Both positive (i.e., sagging) and negative (i.e., hogging) m_x and m_y, as well as positive and negative m_{xy}, are shown in the contour plots. The horizontal and vertical axes indicate the longitudinal and transverse coordinates respectively of the node in a plan view of the bridge, and the values of the colours represent the moments in kN·m/m at each node location. Different contour shapes and values of local bending moments emerge as a result of changes in vehicle paths.

Simulations are extended to other two speeds: 15 and 25 m/s. Tables 6 and 7 summarize the maximum positive and negative moments respectively obtained in the longitudinal and transverse planes and the locations at which they occur.

Table 6. Maximum positive (i.e. sagging) moments (kN·m/m) in longitudinal and transverse planes

	Moments		m_x				m_y				m_{xy}			
			Static	15 m/s	20 m/s	25 m/s	Static	15 m/s	20 m/s	25 m/s	Static	15 m/s	20 m/s	25 m/s
path '1'	Coordinates (m)	X	4.5	4	5	5	4.5	5.5	5	5	0	0	0	0.5
		Y	2	2	2	2	4	4	4	4	5	5	5	5
	Effect (kN·m/m)		67.32	70.44	68.99	72.39	27.13	27.59	28.22	28.31	12.83	14.15	14.17	13.66
path '2'	Coordinates (m)	X	4.5	4	4.5	5	4.5	3.5	4.5	5	0	9	8.5	0
		Y	5.5	5.5	3.5	3.5	5.5	3.5	3.5	3.5	6.5	2.5	2.5	6.5
	Effect (kN·m/m)		60.15	64.59	61.72	65.74	28.25	28.92	29.30	29.60	7.67	8.29	8.08	8.08
path '3'	Coordinates (m)	X	4.5	4.5	4	5	4.5	4.5	3.5	5.5	0	0	0	0
		Y	0	0	0	0	2.5	2.5	2.5	2.5	0	0	0	0
	Effect (kN·m/m)		91.33	95.27	95.00	97.81	20.68	22.32	22.12	22.73	29.36	30.93	30.33	29.87

Table 7. Maximum negative (i.e. hogging) moments (kN·m/m) in longitudinal and transverse planes

	Moments		m_x				m_y				m_{xy}			
			Static	15 m/s	20 m/s	25 m/s	Static	15 m/s	20 m/s	25 m/s	Static	15 m/s	20 m/s	25 m/s
path '1'	Coordinates (m)	X	0	3.5	4.5	4	3	3.5	4.5	4	8.5	9	8.5	9
		Y	4	9	9	9	7.5	7.5	7.5	7.5	5	5	5	5
	Effect (kN·m/m)		-1.85	-2.66	-5.67	-3.83	-1.7	-2.62	-2.88	-2.82	-12.24	-13.42	-15.44	-12.95
path '2'	Coordinates (m)	X	0	0	3	0	0	0	0	0	0	0	9	8.5
		Y	5.5	3.5	0	5.5	5.5	5.5	5.5	5.5	2.5	2.5	6.5	6.5
	Effect (kN·m/m)		-1.85	-2.0	-2.3	-1.93	-1.25	-1.36	-1.39	-1.31	-7.67	-8.59	-8.71	-7.86
path '3'	Coordinates (m)	X	9	4	4.5	4	4.5	5	4.5	0	9	9	9	9
		Y	2.5	0	9	9	6.5	6.5	6.5	5.5	0	0	0	0
	Effect (kN·m/m)		-1.84	-6.87	-8.39	-2.61	-1.26	-6.47	-5.67	-1.31	-27.91	-31.56	-33.34	-28.3

As expected, the maximum positive value of m_x is considerably higher than the positive values of m_y and m_{xy}. While maximum positive m_x occurs around the mid-span section, the maximum positive m_y and maximum positive m_{xy} develop under the wheel path and close to the supports respectively. The exact transverse location of the maximum m_{xy} varies with the vehicle path, i.e., around the middle of the lane for path '2' scenario (Figure 7) and at the bottom corner for the path '3' (Figure 8). As the path of the vehicle moves away from the bridge centreline, the maximum longitudinal bending moment increases both in absolute value and in relative terms compared to the maximum transverse bending moment. While maximum 'static' longitudinal sagging and 'static' twisting moments of 91.33 and 29.36 kN·m/m respectively take place for path '3', a maximum 'static' transverse sagging moment of 28.25 kN·m/m takes place for path '2'. The maximum total longitudinal sagging moment is 35% and 49% higher for path '3' than for paths '1' and '2' respectively. The ratio of maximum longitudinal to maximum transverse sagging moment is 2.22, 2.55 and 4.30 in vehicle paths '2', '1' and '3' respectively.

The maximum negative values of bending moment (Table 7) are considerably smaller than the positive values, but in the case of twisting moment, it is important to calculate both signs given that the maximum twisting could take place in any of the two directions. The ratio of maximum longitudinal sagging to maximum absolute twisting moment is 7.55, 4.69 and 2.93 in vehicle paths '2', '1' and '3' respectively. For path '3', values of twisting moment exceed those of transverse sagging moment. For path '2', absolute 'static' values of negative and positive m_{xy} are naturally equal, but they vary slightly in the dynamic simulations due to randomness of the road profile. Therefore, critical locations of maximum 'static' negative and positive m_{xy} are symmetrical with respect to the bridge centre line.

Table 8 provides values of FDAF for positive m_x, m_y, and m_{xy}. While the maximum total load effect in the numerator of FDAF refers to the worst possible location, the maximum 'static load' effect in the denominator of FDAF refers to a specific location, that here it is taken from

the worst possible static scenario given in Table 6 for positive values and in Table 7 for negative values. The highest FDAF of positive bending moment for the three speeds being tested is 1.09 at 25 m/s, which takes place in path '2' for the longitudinal plane and in path '3' for the transverse plane. A maximum FDAF of 1.10 is found for the positive twisting moment m_{xy} when the vehicle travels on path '1' at speeds of 15 m/s and 20 m/s. A minimum FDAF of 1.01 is found for m_{xy}, when the vehicle is travelling on path '3' at a speed of 25 m/s.

Table 8. FDAF of positive (i.e. sagging) m_x, m_y and m_{xy}

	FDAF of m_x			FDAF of m_y			FDAF of m_{xy}		
Vehicle path	15 m/s	20 m/s	25 m/s	15 m/s	20 m/s	25 m/s	15 m/s	20 m/s	25 m/s
path '1'	1.04	1.02	1.07	1.01	1.04	1.04	1.10	1.10	1.06
path '2'	1.07	1.02	1.09	1.02	1.03	1.04	1.08	1.05	1.05
path '3'	1.04	1.04	1.07	1.07	1.06	1.09	1.05	1.03	1.01

Table 9 provides FDAF of hogging moments, which are generally much higher than those provided in Table 8 for sagging ones. Nevertheless, the total hogging moment remains small given the low values of maximum negative 'static' m_x and m_y (Table 7).

Table 9. FDAF of negative (i.e. hogging) m_x, m_y and m_{xy}

	FDAF of m_x			FDAF of m_y			FDAF of m_{xy}		
Vehicle path	15 m/s	20 m/s	25 m/s	15 m/s	20 m/s	25 m/s	15 m/s	20 m/s	25 m/s
path '1'	1.44	3.06	2.07	1.54	1.69	1.66	1.10	1.26	1.06
path '2'	1.08	1.24	1.04	1.09	1.11	1.05	1.12	1.14	1.02
path '3'	3.73	4.56	1.42	5.13	4.5	1.04	1.13	1.19	1.02

In the case of twisting moments, FDAF of negative m_{xy} should not be overlooked as m_{xy} can reach significant values with both signs. There is a FDAF of 1.26 for negative m_{xy} when the vehicle drives on path '1' at 20 m/s. It is possible to define a global FDAF considering all vehicle paths rather than use a FDAF for each path. For example, global FDAFs of 1.07, 1.05 and 1.14 can be obtained for longitudinal sagging, transverse sagging, and twisting moments respectively. The next section extends the analysis of moments from the longitudinal and

transverse planes to any plane orientation. This analysis aims to stablish the bridge moment capacity needed to withstand the applied total ('static' + 'dynamic') moment regardless of the plane orientation.

4. Bending Moments Acting at any Plane

A slab deck has infinite points, and infinite number of planes passing through each point. This section establishes the magnitude of the highest moments, and the node location and plane orientation at which they occur. Figure 9 shows a plan view of the moments acting on a portion of the slab delimited by three edges: BC of length *L*, AB of length $L\cos\theta$, and AC of length $L\sin\theta$. AB, AC and BC are contained in planes of normal *x*, *y* and *n* respectively, and θ is the angle between *x*- and *n*- directions. On each of these planes, there are two moments: a bending moment (where the subscript denotes the direction of the normal to the plane on which the moment is acting) that produces normal stresses, and a twisting moment (where the first and second subscripts represent the direction of the normal to the plane on which the moment is acting, and the direction of the shear stresses respectively) that produces shear stresses.

By imposing equilibrium of moments in the *n*-direction (Equation (10)) and in a direction perpendicular to *n* (Equation (11)), it is possible to obtain the bending moment, m_n, and twisting moment, m_{nt}, per unit breadth acting on a plane of normal *n* [4,26].

$$m_n = m_x \cos^2\theta + m_y \sin^2\theta - 2\, m_{xy} \sin\theta \cdot \cos\theta \quad (10)$$

$$m_{nt} = (m_x - m_y) \sin\theta \cdot \cos\theta + m_{xy}(\cos^2\theta - \sin^2\theta) \quad (11)$$

where θ is the angle that the normal to the plane (*n*) makes with the horizontal *x*-axis.

m_x, m_y and m_{xy} obtained in Section 3 are substituted into Equation (10) to calculate m_n for every node of the FE model. θ values are varied in 1 degree increment from 0 to 360°. The maximum

positive (Max_m_n, i.e., sagging) and minimum negative (Min_m_n, i.e., hogging) of 'static' and total (15, 20 and 25 m/s) values of m_n are plotted versus θ in Figure 10(a) for the vehicle travelling on path '1'. Similarly, moments m_x, m_y and m_{xy} are replaced into Equation (11) to obtain the maximum (Max_m_{nt}) and minimum (Min_m_{nt}) twisting moments per unit breadth for every node. The latter are shown in Figure 10(b) for the vehicle travelling on path '1'. Highest values of Max_m_n take place at longitudinal planes (θ values of 0°, 180° and 360° - points labelled 'S1' in the figure -), whereas minimum values of Max_m_n are found at transverse planes (θ values of 90° and 270° - points labelled 'S2'-). Minimum values of Min_m_n develop for planes at 45° with horizontal and vertical planes (θ values of 45° and 225 - points labelled 'H1' -, and 225° and 315° - points labelled 'H2' -). Figure 10(b) shows that the most positive and most negative twisting moments also occur in planes at 45° with horizontal and vertical planes (θ values of 45° and 225° for largest positive m_{nt} - points labelled 'T1' -, and θ values of 135° and 315° for largest negative m_{nt} - points 'T2' -). In summary, longitudinal and transverse bending moments are the maximum and minimum bending moments respectively. Besides, critical twisting moments occur in planes at 45° with respect to the longitudinal and transverse planes.

Figure 11 shows a 3-dimensional plot that locates the FE node that leads to maximum 'static' bending moments (negative 'Min_m_n' labelled as purple triangles and positive 'Max_m_n' labelled as red circles) and maximum 'static' twisting moments (maximum 'Max_m_{nt}' labelled as black squares and minimum 'Min_m_{nt}' labelled as green crosses) for each plane orientation θ. The locations holding these maximum and minimum moments vary for each θ value, but are placed predominantly around midspan for Max_m_n, and spread throughout the bridge for Min_m_n, Max_m_{nt} and Min_m_{nt}. The largest sagging moment occur in a longitudinal plane at or near midspan, where the bending curvature of the deflected shape is highest. Bending curvatures in other directions also increase the closer to midspan. For twisting and hogging

moments, the critical locations for each plane orientation are more variable due to the influence of local effects. Maximum hogging appears in the half of the bridge where the vehicle is not travelling, and largest absolute twisting moments tend to be found near the edges at midspan and in the corners.

The coordinates of the critical locations cannot be clearly visualized in the 3-dimensional graph of Figure 11. For this reason, horizontal sections for θ orientations equal to 45°, 90°,135° and 180° holding maximum 'static' and total moments are obtained. Figure 12 provides the X- (horizontal axis, i.e. bridge span length) and Y- (vertical axis, i.e. bridge width) coordinates of the critical locations for the four selected orientations, and how they vary with speed. For instance, Figures 12(b) for 15 m/s and 12(d) for 25 m/s show 4 red circles which represent the critical locations holding the maximum sagging for plane orientations equal to 45°, 90°, 135° and 180°. However, Figures 12(a) ('static') and 12(c) for 20 m/s show 6 red circles, given that the maximum sagging is reached at more than one critical location for some orientations. Here, the points 'S1' (at Θ values of 0°, 180° and 360° in Figure 10(a)), 'S2' (at Θ values of 90° and 270°), 'H1' (at Θ values of 45° and 225°) and 'H2' (at Θ values of 135° and 315°) represent the locations with maximum and minimum sagging and hogging moments. Point 'T1' corresponds to the coordinates of the largest positive twisting moment (Max_m_{nt} at θ = 45° and 225° in Figure 10(b)) and 'T2' to the largest negative twisting moment (Min_m_{nt} at θ = 135° and 225° in Figure 10(b)). It can be seen that maximum sagging moments develop near the mid-span section in the half of the bridge traversed by the vehicle. The largest sagging moment for path '1' takes place at coordinates X = 5 m and Y = 2 m for a speed of 25 m/s (point S1 in Figure 12(d)). The 'dynamic' component of the total response will not reach a peak simultaneously with the 'static' component at midspan, except for a critical speed causing a high DAF. As a result, the locations of maximum total sagging moments (Figures 12(b), (c)

and (d)) appear more scattered than the locations of maximum 'static' sagging moments (Figure 12(a)).

Tables 10, 11 and 12 provide the largest values associated to the four θ in Figure 12 (Max_m_n at 'S1', Max_m_n at 'S2', Min_m_n at 'H1', Min_m_n at 'H2', Max_m_{nt} at 'T1' and Min_m_{nt} at 'T2') taking into account all loading scenarios.

Table 10. Maximums and minimums of sagging bending moments (kN·m/m)

	Theta		S1				S2			
			Static	15	20	25	Static	15	20	25
path '1'	Coor.	X	4.5	4	5	5	4.5	5.5	5	5
		Y	2	2	2	2	4	4	4	4
	Effect		67.33	70.46	68.99	72.39	27.13	27.59	28.22	28.31
path '2'	Coor.	X	4.5	4	4.5	5	4.5	3.5	4.5	5
		Y	3.5	5.5	3.5	3.5	5.5	3.5	3.5	3.5
	Effect		60.15	64.59	61.72	65.74	28.26	28.92	29.30	29.6
path '3'	Coor.	X	4.5	4.5	4	5	5	4.5	6	5
		Y	0	0	0	0	2.5	2.5	2.5	2.5
	Effect		91.33	95.27	95	97.81	20.68	22.32	22.10	22.92

Table 11. Maximums and minimums of hogging normal moments (kN·m/m)

	Theta		H1				H2			
			Static	15	20	25	Static	15	20	25
path '1'	Coor.	X	0	0	0	0	9	9	9	9
		Y	5	5	5	5	5	5	5	5
	Effect		-12.76	-14.04	-14.14	-13.61	-12.19	-13.35	-15.37	-12.87
path '2'	Coor.	X	0	9	9	0	0	0	9	0
		Y	6.5	2.5	2.5	6.5	2.5	2.5	6.5	2.5
	Effect		-7.57	- 8.18	-7.92	-7.95	-7.56	- 8.41	-8.60	-7.76
path '3'	Coor.	X	0	0	0	0	9	9	9	9
		Y	0	0	0	0	0	0	0	0
	Effect		-25.71	-27.31	-26.76	-26.62	-25.04	-28.91	-30.12	-25.55

Table 12. Maximum and minimum twisting moments (kN·m/m)

	Theta		T1				T2			
			Static	15	20	25	Static	15	20	25
path '1'	Coor.	X	4.5	4	4	5	4.5	4	4	5
		Y	0	0	0	0	0	0	0	0
	Effect		30.07	32.02	32.06	32.75	-30.07	-32.02	-32.06	-32.75
path '2'	Coor.	X	4.5	4	4.5	4.5	4.5	4	4.5	4.5
		Y	1	0.5	0.5	0.5	1	0.5	0.5	0.5
	Effect		20.81	23.29	21.99	23.18	-20.81	-23.29	-21.99	-23.18
path '3'	Coor.	X	4.5	4.5	3.5	5	4.5	4.5	3.5	5
		Y	0	0	0	0	0	0	0	0
	Effect		46.28	47.99	47.79	49.31	-46.28	-47.99	-47.79	-49.31

Table 10 shows that the highest values are reached by the positive bending moment (i.e. sagging moment) at 'S1' ($\theta = 0°$, 180° and 360°). The longitudinal coordinate where maximum m_n develops extend over a region near the mid-length of the bridge and the corresponding transverse coordinates are determined by the vehicle path. Table 11 shows that negative bending moment (i.e. hogging moment) Min_m_n at 'H1' takes place at the first support of the bridge, however, it develops at the second support when the vehicle travels along path '2' at speeds of 15 m/s and 20 m/s. Hogging moment Min_m_n at 'H2' takes place at the second support of the bridge, however, it develops at the first support when the vehicle is statically positioned along path '2' and when the vehicle travels along this path at speeds of 15 m/s and 25 m/s.

In Table 12, as expected, maximum (Max_m_{nt} at 'T1') and minimum (Min_m_{nt} at 'T2') twisting moments have opposite signs and equal absolute values. Max_m_{nt} at 'T1' and Min_m_{nt} at 'T2' are located on the bridge edges. Max_m_{nt} at 'T1' and Min_m_{nt} at 'T2' are, however, present a bit further from the edge of the bridge when path '2' is pursued by the vehicle. Furthermore, Max_m_{nt} at 'T1', Min_m_{nt} at 'T2' and the largest values of bending moments Max_m_n at 'S1' are present at the same places when the vehicle is statically positioned along path '3' and when it travels along this path at speeds of 15 and 25 m/s.

Table 13 gives the FDAF for sagging moments *Max_*m_n at ‘S2’ and *Max_*m_n at ‘S1’.

Table 13. FDAF of sagging bending moments

FDAF	FDAF of m_n at ‘S1’			FDAF of m_n at ‘S2’		
Path	15 m/s	20 m/s	25 m/s	15 m/s	20 m/s	25 m/s
path ‘1’	1.04	1.02	1.07	1.01	1.04	1.04
path ‘2’	1.07	1.02	1.09	1.02	1.03	1.04
path ‘3’	1.04	1.04	1.07	1.07	1.06	1.09

Table 14 presents the FDAF for hogging moments *Min_*m_n at ‘H1’ and *Min_*m_n at ‘H2’.

Table 14. FDAF of hogging bending moments

FDAF	FDAF of m_n at ‘H1’			FDAF of m_n at ‘H2’		
Path	15 m/s	20 m/s	25 m/s	15 m/s	20 m/s	25 m/s
path ‘1’	1.1	1.11	1.07	1.09	1.26	1.05
path ‘2’	1.08	1.05	1.05	1.11	1.13	1.02
path ‘3’	1.06	1.041	1.04	1.15	1.20	1.02

Table 15 gives the FDAF for twisting moments *Max_*m_{nt} at ‘T1’ and *Min_*m_{nt} at ‘T2’.

Table 15. FDAF of maximum and minimum twisting moments (kN·m/m)

FDAF	FDAF of m_{nt} at ‘T1’			FDAF of m_{nt} at ‘T2’		
Path	15 m/s	20 m/s	25 m/s	15 m/s	20 m/s	25 m/s
path ‘1’	1.06	1.06	1.09	1.06	1.06	1.09
path ‘2’	1.12	1.05	1.11	1.12	1.05	1.11
path ‘3’	1.03	1.03	1.06	1.03	1.03	1.06

The majority of FDAF values for twisting moments and hogging moments are larger than those of sagging moments (*Max_*m_n at ‘S1’ and ‘S2’). The largest FDAF value is 1.26 for hogging bending moment *Min_*m_n at ‘H2’ when the vehicle is travelling on path ‘1’ at 20 m/s.

On the one hand, the critical sagging moment m_n at ‘S1’ in Table 13 has the same associated FDAFs than m_x in Table 8, the reason being that the plane with largest sagging moment is the longitudinal plane. Similarly, the sagging moment m_n at ‘S2’ refers to the transverse plane, and consequently, it has the same FDAFs as m_y in Table 8. On the other hand, FDAFs at ‘T1’ and ‘T2’ (at 45° with vertical and horizontal planes) in Table 15 are different from FDAFs for m_{xy} in Table 8, given that they refer to different planes. Largest FDAF associated to m_{nt} ($\theta = 45°$) is 1.12.

The location, amount and strength of steel reinforcement and the section dimensions will determine the moment capacity of the bridge in kN·m/m. The latter must have a value exceeding the applied moment. If orthogonal reinforcement was to be provided in X- and Y-directions, i.e., m_x* and m_y*, it is necessary to ensure that moment capacities in other directions are also sufficiently large to prevent failure. For this purpose, the moment capacity at any plane m_n* can be estimated from replacing m_n by m_n*, m_x by m_x*, m_y by m_y* and m_{xy} by 0 in Equation (10), leading to '$m_x^* = m_x + |m_{xy}|$' and '$m_y^* = m_y + |m_{xy}|$'. For example, the values of the sagging capacities in longitudinal and transverse planes needed to withstand moments caused by the vehicle travelling in path '1' at 25 m/s are estimated next for the point X = 5 m and Y = 2 m (where the maximum longitudinal bending moment of m_x = 72.39 kN·m/m takes place). The contour plot in Figure 13(a) illustrates the variation of bending moment at this point with plane orientation for each point in time (t = 0 seconds when the first axle of the truck is at the entrance support). A concentration of high bending moments takes place for t = 0.57 seconds. Figure 13(b) shows how the capacities '$m_x^* = m_x + |m_{xy}|$' and '$m_y^* = m_y + |m_{xy}|$' required at the point (X = 5 m, Y = 2 m) vary with m_x, m_y and m_{xy} for each instant. Maximum bending capacities of m_x* = 73.37 kN·m/m and of m_y*= 27.33 kN·m/m are necessary to withstand the moments experienced at t = 0.57 seconds. While only the action of the vehicle is investigated in this paper, combinations of actions (i.e., including self-weight) need to be taken into consideration when calculating Max_m_n in a practical situation. Other vehicle paths and a full range of potential speeds (i.e., including critical speeds causing highest DAFs) also need to be checked to ensure m_x* and m_y* cover all possible failure scenarios.

5. Conclusions

This paper has investigated how a moving vehicle affects the 'static' and total moment acting on any plane orientation of a short-span straight solid slab bridge. The crossing of a 5-axle

articulated truck over a FE plate model of the bridge on a class 'A' road carpet has been simulated for nine loading scenarios including three vehicle speeds (15, 20 and 25 m/s) and three transverse paths. For all scenarios, positive and negative bending and twisting moments per unit breadth have been obtained in longitudinal and transverse planes. It has been found that longitudinal sagging (m_x) exhibits considerably larger values than transverse sagging (m_y) or twisting (m_{xy}). Maximum values occur most frequently over the middle portion of the bridge for m_x, over the bridge centreline for m_y, and at the bridge edges for m_{xy}. Bridge codes such as the Eurocode, propose traffic load models with built-in DAFs that quantify the increase that the total response experiences as a result of dynamic VBI. For a two-lane 9 m bridge, this DAF value is 1.26 [21]. However, built-in DAFs are necessarily conservative and do not allow for changes in DAF for different moments. For the bridge scenarios under investigation, FDAF of m_x and m_y in sagging have had similar values with a maximum of 1.09 (vehicle travelling at 25 m/s, either along middle of the bridge for worst m_x or partially on the shoulder for worst m_y), but a maximum FDAF of negative m_{xy} have reached 1.26 (vehicle travelling at 20 m/s along the middle of the lane).

Furthermore, total ('static' + 'dynamic') bending (m_n) and twisting (m_{nt}) moments acting on any plane of normal n have been analysed. From the point of view of sagging moments, the plane orientations leading to largest values have taken place at longitudinal planes, i.e., largest $Max\_m_n = m_x$. The plane orientations leading to smallest values of Max_m_n have occurred at transverse planes, i.e., smallest $Max\_m_n = m_y$. Largest values of hogging and twisting moments have developed at 45° with respect to longitudinal and transverse planes. Even though bending moments will be largest at longitudinal planes, this paper has shown that bending failure may occur at orientations other than longitudinal. Therefore, the maximum total applied moment (Max_m_n) must be calculated and compared to the available moment capacity of the bridge (m_n*) for every plane orientation. An accurate assessment taking into account

these subtleties is clearly justified if an existing bridge could be saved from unnecessary strengthening or replacing.

ACKNOWLEDGEMENTS

The authors wish to express their gratitude for the financial support received from Al-Anbar University and Iraqi ministry of higher education towards this research.

References

[1] DIVINE. Dynamic interaction of heavy vehicles with roads and bridges, Canada. DIVINE Concluding Conference; OCED; Ottawa; Technical report; 1997.

[2] OBrien EJ, Cantero D, Enright B, González A. Characteristic Dynamic Increment for extreme traffic loading events on short and medium span highway bridges. Eng Struct 2010;32:3827–35.

[3] Tarmac. Prestressed beams technical guide 2009.

[4] Wood RH. The Reinforcement of Slabs in Accordance with a Pre-Determined Field of Moments. Concrete 1968;2:69–76.

[5] Zararis PD. State of Stress in RC Plates under Service Conditions. J Struct Eng 1986;112:1908–27.

[6] Zararis PD. Failure Mechanisms in R/C Plates Carrying In-Plane Forces. J Struct Eng 1988;114:553–74.

[7] Ghoneim MG, MacGregor JG. Behavior of Reinforced Concrete Plates Under Combined Inplane and Lateral Loads. Struct J 1994;91:188–97.

[8] Ghoneim MG, Macgregor JG. Prediction of the Ultimate Strength of Reinforced Concrete Plates Under Combined Inplane and Lateral Loads. Struct J 1994;91:688–96.

[9] Ghoneim MG, McGregor JG. Tests of Reinforced Concrete Plates Under Combined Inplane and Lateral Loads. Struct J 1994;91:19–30.

[10] Frýba L. Vibration of solids and structures under moving loads. Groningen, The Netherlands: Noordhoff International Publishing; 1972.

[11] Bakht B, Pinjarkar S. G. Dynamic testing of highway bridges—A review. Transportation Research Record 1223, Transportation Research Board, Washington, DC, 93–100. 1989.

[12] Inbanathan MJ, Wieland M. Bridge Vibrations Due to Vehicle Moving Over Rough Surface. J Struct Eng 1987;113:1994–2008.

[13] Wang W, Deng L, Asce M. Impact Factors for Fatigue Design of Steel I-Girder Bridges Considering the Deterioration of Road Surface Condition. J Bridg Eng 2016;21:04016011.

[14] Park YS, Shin DK, Chung TJ. Influence of road surface roughness on dynamic impact factor of bridge by full-scale dynamic testing. Can J Civ Eng 2005;829:825–9.

[15] Senthilvasan J, Thambiratnam D., Brameld G. Dynamic response of a curved bridge under moving truck load. Eng Struct 2002;24:1283–93.

[16] Moghimi H, Ronagh HR. Impact factors for a composite steel bridge using non-linear dynamic simulation. Int J Impact Eng 2008;35:1228–43.

[17] Rezaiguia A, Ouelaa N, Laefer DFF, Guenfoud S. Dynamic amplification of a multi-span, continuous orthotropic bridge deck under vehicular movement. Eng Struct 2015;100:718–30.

[18] Mohammed O, Cantero D, González A, Al-Sabah S. Dynamic amplification factor of continuous versus simply supported bridges due to the action of a moving load, Civil engineering research in Ireland (CERI 2014) , Queen's Univ, Belfast, 28-29 August, 2014. 2014-08-29: 2014.

[19] Pesterev AV, Bergman LA, Tan CA, Yang B. Application of the pothole DAF method to vehicles traversing periodic roadway irregularities. J Sound Vib 2005;279:843–55.

[20] Cantero D, González A, OBrien EJ. Maximum dynamic stress on bridges traversed by moving loads. Proc ICE - Bridg Eng 2009;162:75–85.

[21] González A, Cantero D, OBrien EJ. Dynamic increment for shear force due to heavy vehicles crossing a highway bridge. Comput Struct 2011;89:2261–72.

[22] Zienkiewicz OC, Taylor RL, Zhu JZ, OCZ, Rlt, Jzz. The Finite Element Method Set. Elsevier; 2005.

[23] Reddy JN. Energy Principles and Variational Methods in Applied Mechanics. John Wiley & Sons; 2002.

[24] Bonger FK, Fox RL, Schmit LA. The generation of inter-element-compatible stiffness and mass matrices by the use of interpolation formulas. Proceeding's 1st Conf. matrix methods Struct. Mech. Air Force Inst Tech, Wright Patterson A.F. Base, Ohio, 397-443, 1965.

[25] Rowley C. Moving force identification of axle forces in bridges. PhD thesis. School Civ Eng, University College Dublin, Ireland, 2007.

[26] OBrien EJ, Keogh D, O,Connor A. Bridge deck Analysis. CRC Press ; 2015.

[27] Li YC. Factors affecting the dynamic interaction of bridges and vehicle loads. PhD Thesis, Dep Civ Eng, University College Dublin,Ireland, 2006.

[28] Clough RW and Penzien J. Dynamics of structures. 2nd editio. McGraw-Hil; 1993.

[29] Cantero D, González A, OBrien EJ. Comparison of bridge dynamic amplification due to articulated 5-axle trucks and large cranes. Balt J Road Bridg Eng 2011;6:39–47.

[30] Cebon D. Handbook of vehicle-road interaction. Swets & Zeitlinger Lisse, The Netherlands; 1999.

[31] González A, OBrien EJ, Cantero D, Li Y, Dowling J, Žnidarič A. Critical speed for the dynamics of truck events on bridges with a smooth road surface. J Sound Vib 2010;329:2127–46. doi:10.1016/j.jsv.2010.01.002.

[32] Deng L, Cai CSS. Development of dynamic impact factor for performance evaluation of existing multi-girder concrete bridges. Eng Struct 2010;32:21–31.

[33] Kim C-W, Kawatani M, Kwon Y-R. Impact coefficient of reinforced concrete slab on a steel girder bridge. Eng Struct 2007;29:576–90.

[34] Broquet C, Bailey SF, Fafard M, Brühwiler E. Dynamic behavior of deck slabs of concrete road bridges. J Bridg Eng, 9 (2) (2004), pp. 137–146.

[35] Huang DZ, Wang TL, Shahawy M. Dynamic behavior of horizontally curved I-girder bridges. Comput Struct 1995;57:703–14.

[36] Huang DZ, Wang TL, Shahawy M. Impact analysis of continuous multigirder bridges due to moving vehicles. J Struct Eng 1992;118:3427–43.

[37] Cebon D, Newland DE. Artificial generation of road surface topography by the inverse FFT method. Veh Syst Dyn 1983;12:160–5.

[38] ISO 8608:1995, Mechanical Vibration-road Surface Profiles-reporting of Measured Data', International Standards Organisation. 1995.

[39] Keenahan J, OBrien EJ, McGetrick PJ, Gonzalez A. The use of a dynamic truck-trailer drive-by system to monitor bridge damping. Struct Heal Monit 2013;13:143–57.

[40] Harris NK, OBrien EJ, González A. Reduction of bridge dynamic amplification through

adjustment of vehicle suspension damping. J Sound Vib 2007;302:471–85.

[41] Sayers M, Karamihas S. Interpretation of road roughness profile data. Tech rep, Univ of Michigan Transportation Research Institute (UMTRI) Report 96–19, 1996.

[42] Green MF, Cebon D. Dynamic interaction between heavy vehicles and highway bridges. Comput Struct 1997;62:253–64.

[43] Cantero D, OBrien EJ, González A. Modelling the vehicle in vehicle-infrastructure dynamic interaction studies. Proc Inst Mech Eng Part K J Multi-Body Dyn 2010;224:243–8.

Figure captions:

Figure 1. Moments acting on longitudinal and transverse planes of plate element with four nodes

Figure 2. General vehicle model sketch: (a) Side view, (b) Front view (Symbols defined in Table 3)

Figure 3. Road profile carpet

Figure 4. Plan view showing location of vehicle paths on bridge plate model

Figure 5: Longitudinal bending moment per unit breadth m_x: (a) Total and static m_x versus truck location for node at 3.5 m from left edge of the bridge, (b) Total and static m_x versus truck location for node at right edge of the bridge, (c) Envelope of maximum static and total m_x at section A-A.

Figure 6. Envelope of maximum positive and negative moments for vehicle travelling on path '1' of the bridge at 20 m/s: (a) Maximum static positive m_x (kN·m/m), (b) Maximum total positive m_x (kN·m/m), (c) Maximum static negative m_x (kN·m/m), (d) Maximum total negative m_x (kN·m/m), (e) Maximum static positive m_y (kN·m/m), (f) Maximum total positive m_y (kN·m/m), (g) Maximum static negative m_y (kN·m/m), (h) Maximum total negative m_y (kN·m/m), (i) Maximum static positive m_{xy} (kN·m/m), (j) Maximum total positive m_{xy} (kN·m/m), (k) Maximum static negative m_{xy} (kN·m/m), (l) Maximum total negative m_{xy} (kN·m/m)

Figure 7. Envelope of maximum positive and negative moments for vehicle travelling on path '2' of the bridge at 20 m/s: (a) Maximum static positive m_x (kN·m/m), (b) Maximum total positive m_x (kN·m/m), (c) Maximum static negative m_x (kN·m/m), (d) Maximum total negative m_x (kN·m/m), (e) Maximum static positive m_y (kN·m/m), (f) Maximum total positive m_y (kN·m/m), (g) Maximum static negative m_y (kN·m/m), (h) Maximum total negative m_y (kN·m/m), (i) Maximum static positive m_{xy} (kN·m/m), (j) Maximum total positive m_{xy} (kN·m/m), (k) Maximum static negative m_{xy} (kN·m/m), (l) Maximum total negative m_{xy} (kN·m/m)

Figure 8. Envelope of maximum positive and negative moments for vehicle travelling on path '3' of the bridge at 20 m/s: (a) Maximum static positive m_x (kN·m/m), (b) Maximum total positive m_x (kN·m/m), (c) Maximum static negative m_x (kN·m/m), (d) Maximum total

negative m_x (kN·m/m), (e) Maximum static positive m_y (kN·m/m), (f) Maximum total positive m_y (kN·m/m), (g) Maximum static negative m_y (kN·m/m), (h) Maximum total negative m_y (kN·m/m), (i) Maximum static positive m_{xy} (kN·m/m), (j) Maximum total positive m_{xy} (kN·m/m), (k) Maximum static negative m_{xy} (kN·m/m), (l) Maximum total negative m_{xy} (kN·m/m)

Figure 9. Plan view of moments acting on a plate slice

Figure 10. Static and total moments for vehicle travelling at 15, 20 and 25 m/s on path '1' of the bridge: (a) Min_m_n and Max_m_n versus θ, (b) Max_m_{nt} and Min_m_{nt} versus θ

Figure 11. 3-D plot of critical locations of static moments (Max_m_n , Min_m_n, Max_m_{nt} and $Min\_m_{nt)}$ for each angle θ when vehicle travels on path '1'

Figure 12. Critical locations of Max_m_n, Min_m_n, Max_m_{nt} and Min_m_{nt} for vehicle travelling on path '1': (a) Static, (b) Total at 15 m/s, (c) Total at 20 m/s, (d) Total at 25 m/s

Figure 13. Moments acting on point of coordinates (X = 5 m,Y = 2 m) due to the vehicle travelling along path '1' at 25 m/s: (a) Bending moment m_n versus time and plane orientation (0 to 360 degrees), (b) m_x, m_y, m_{xy}, m_x* and m_y* versus time

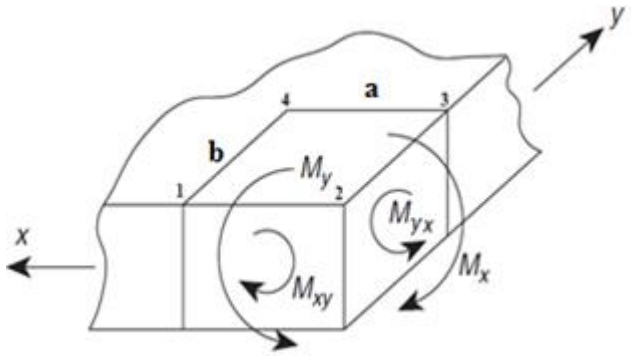

Figure 1. Moments acting on longitudinal and transverse planes of plate element with four nodes

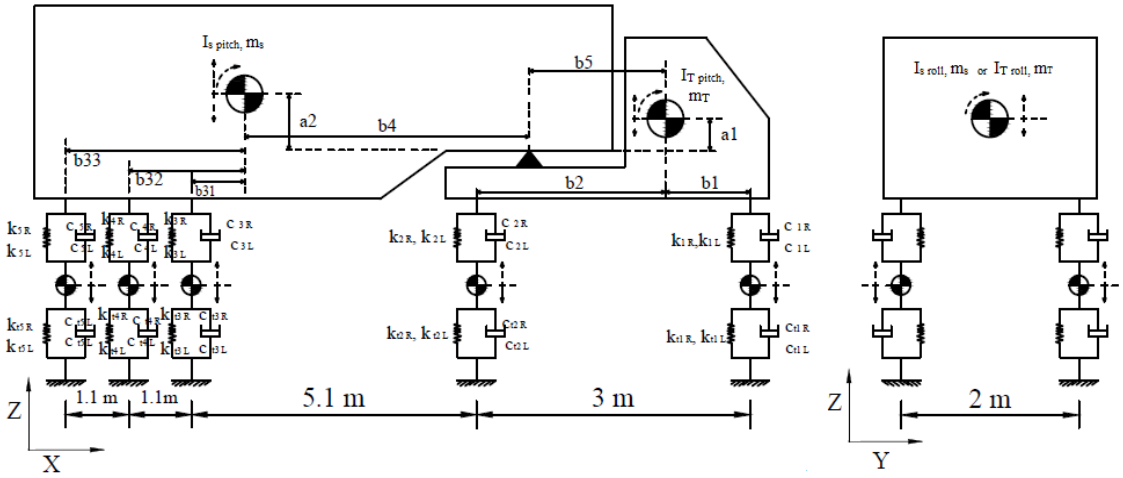

(a) (b)

Figure 2. General vehicle model sketch: (a) Side view, (b) Front view (Symbols defined in Table 3)

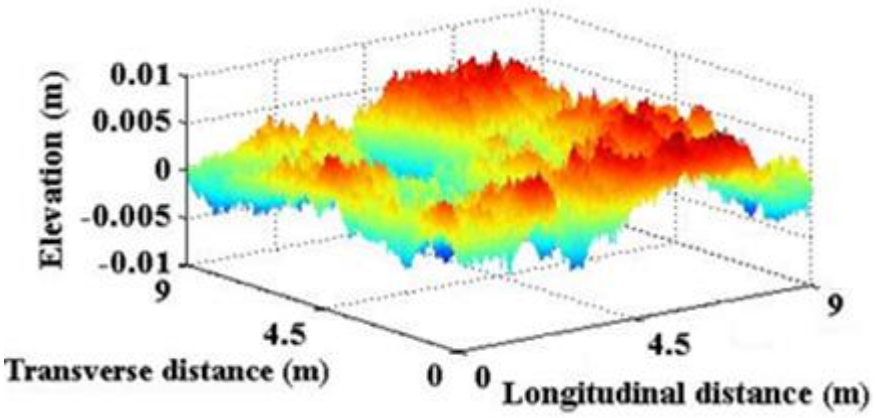

Figure 3. Road profile carpet

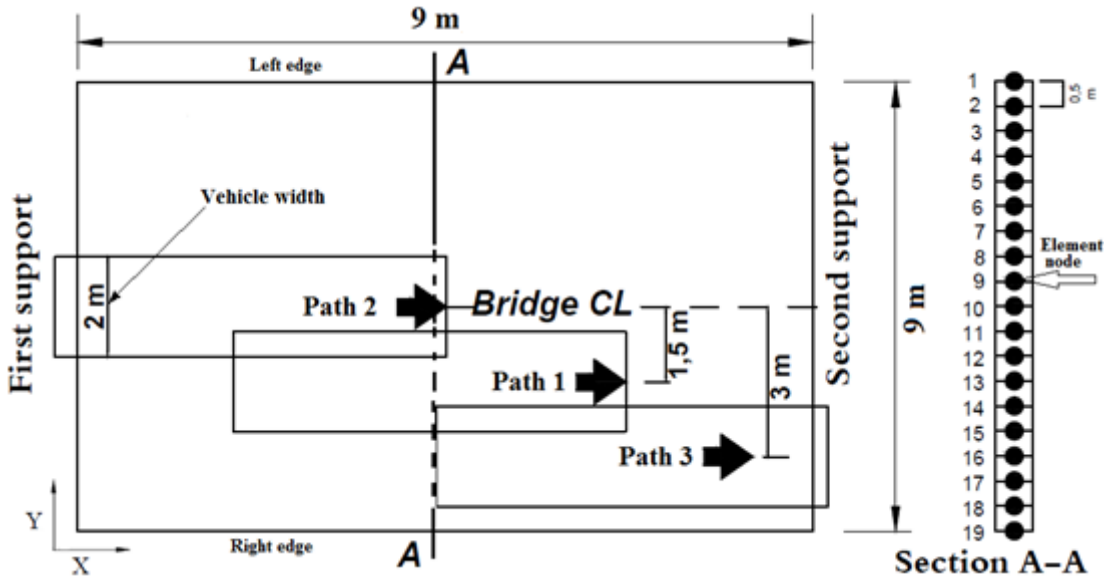

(➔) Centreline of the vehicle

Figure 4. Plan view showing location of vehicle paths on bridge plate model

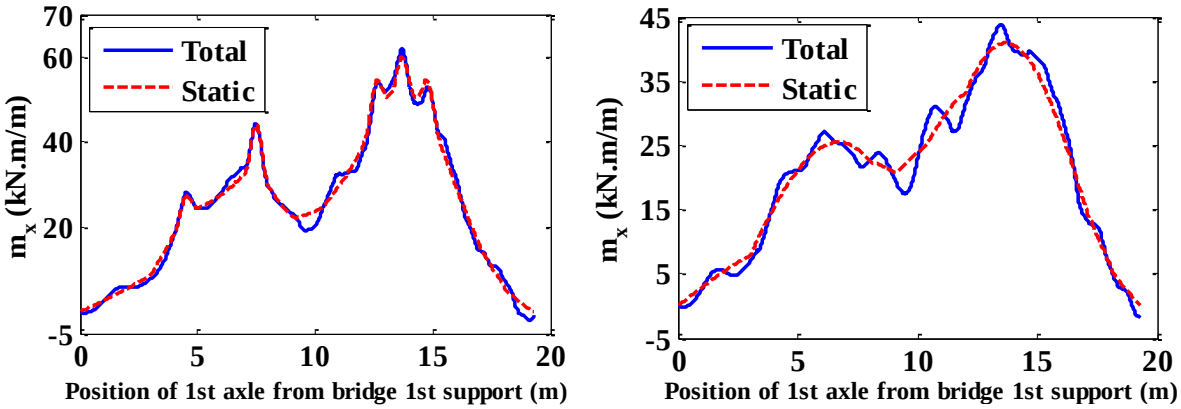

(a) (b)

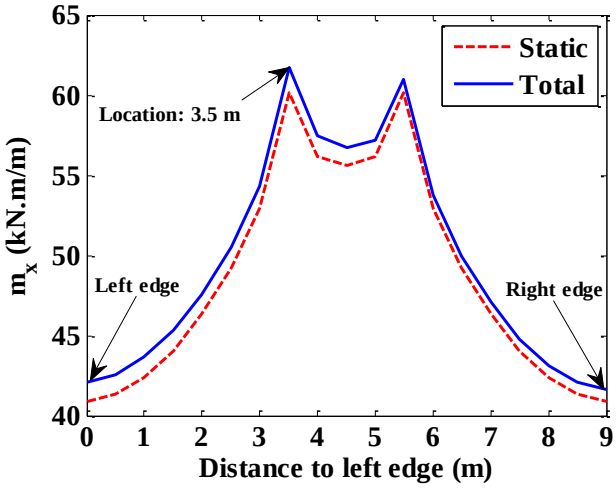

(c)

Figure 5. Longitudinal bending moment per unit breadth m_x: (a) Total and static m_x versus truck location for node at 3.5 m from left edge of the bridge, (b) Total and static m_x versus truck location for node at right edge of the bridge, (c) Envelope of maximum static and total m_x at section A-A.

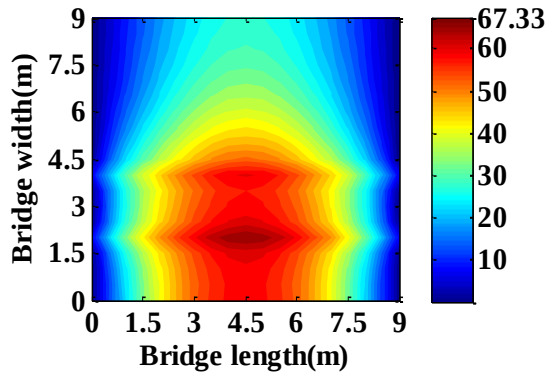
Bridge width(m)
Bridge length(m)
0 1.5 3 4.5 6 7.5 9
67.33
60
50
40
30
20
10

(a)

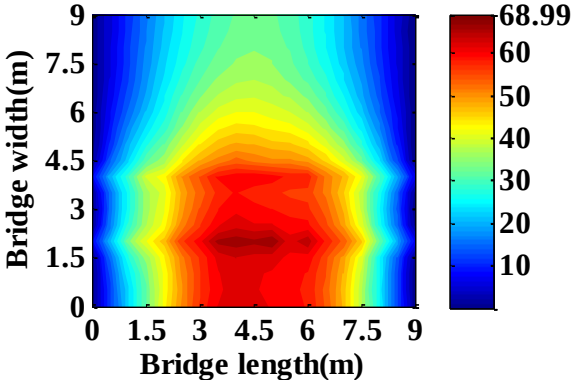
Bridge width(m)
Bridge length(m)
0 1.5 3 4.5 6 7.5 9
68.99
60
50
40
30
20
10

(b)

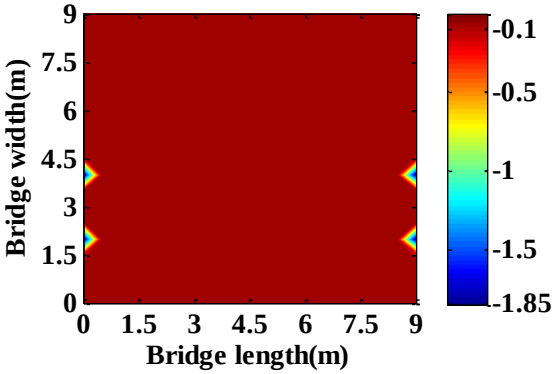
Bridge width(m)
Bridge length(m)
0 1.5 3 4.5 6 7.5 9
-0.1
-0.5
-1
-1.5
-1.85

(c)

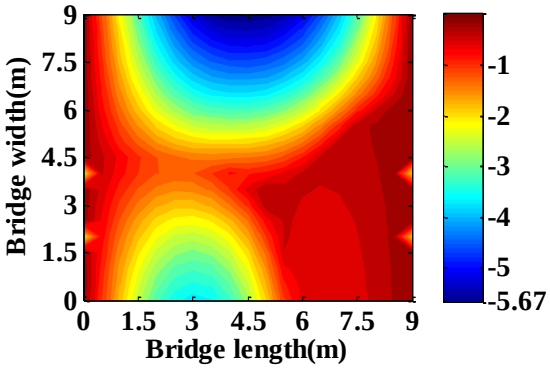
Bridge width(m)
Bridge length(m)
0 1.5 3 4.5 6 7.5 9
-1
-2
-3
-4
-5
-5.67

(d)

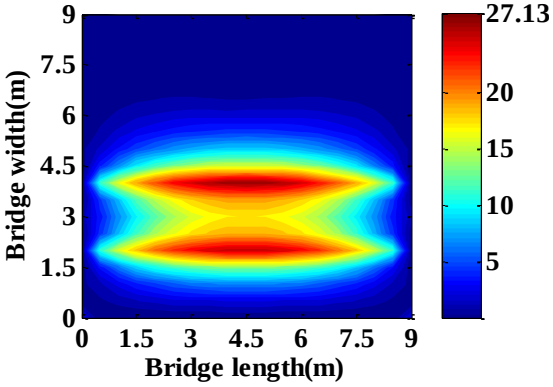
Bridge width(m)
Bridge length(m)
0 1.5 3 4.5 6 7.5 9
27.13
20
15
10
5

(e)

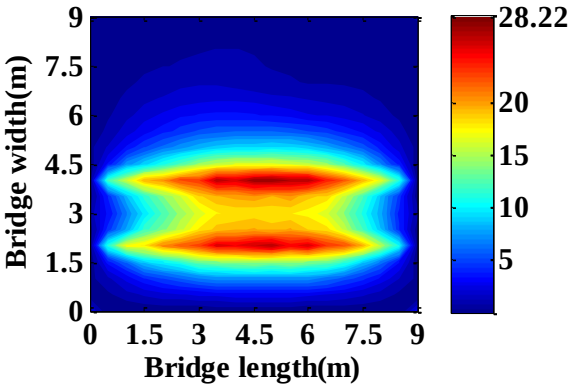
Bridge width(m)
Bridge length(m)
0 1.5 3 4.5 6 7.5 9
28.22
20
15
10
5

(f)

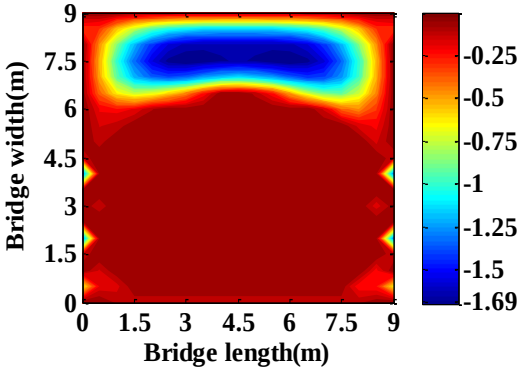
Bridge width(m)
Bridge length(m)
0 1.5 3 4.5 6 7.5 9
-0.25
-0.5
-0.75
-1
-1.25
-1.5
-1.69

(g)

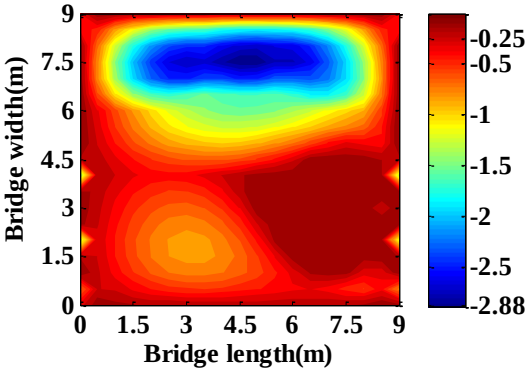
Bridge width(m)
Bridge length(m)
0 1.5 3 4.5 6 7.5 9
-0.25
-0.5
-1
-1.5
-2
-2.5
-2.88

(h)

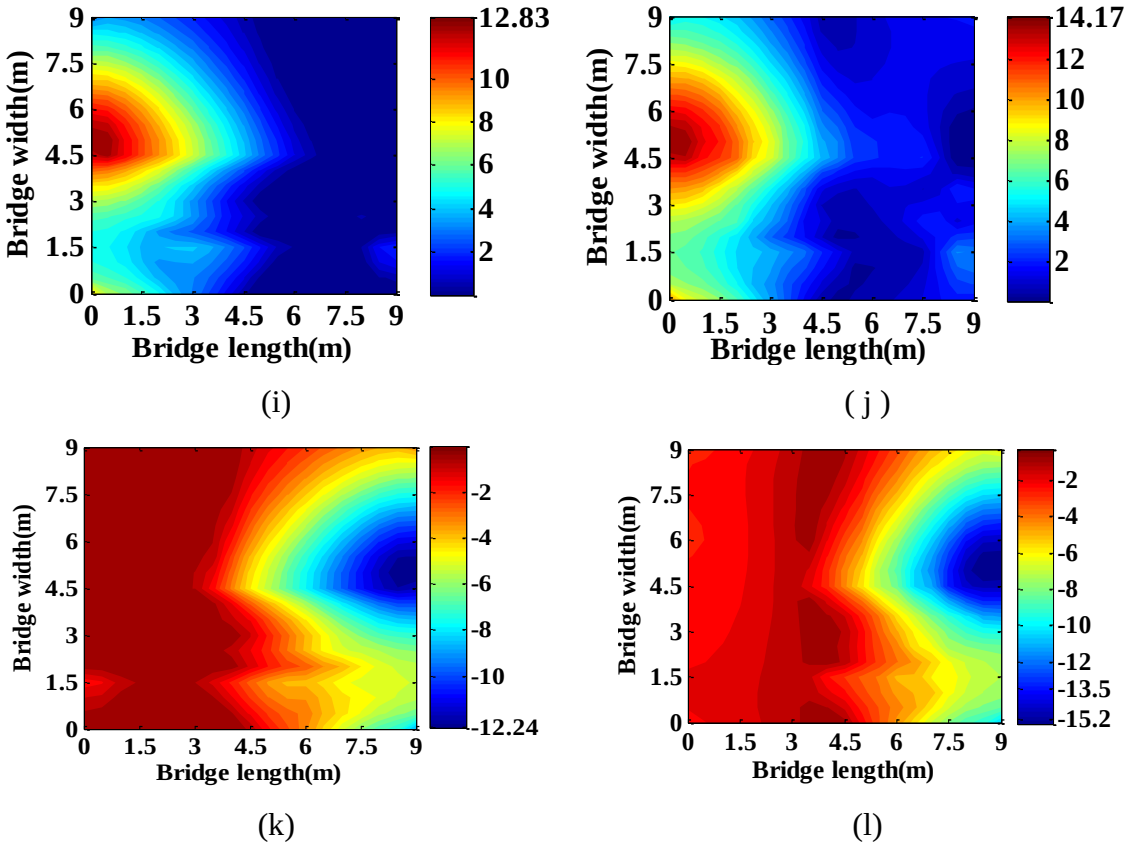

Figure 6. Envelope of maximum positive and negative moments for vehicle travelling on path '1' of the bridge at 20 m/s: (a) Maximum static positive m_x (kN·m/m), (b) Maximum total positive m_x (kN·m/m), (c) Maximum static negative m_x (kN·m/m), (d) Maximum total negative m_x (kN·m/m), (e) Maximum static positive m_y (kN·m/m), (f) Maximum total positive m_y (kN·m/m), (g) Maximum static negative m_y (kN·m/m), (h) Maximum total negative m_y (kN·m/m), (i) Maximum static positive m_{xy} (kN·m/m), (j) Maximum total positive m_{xy} (kN·m/m), (k) Maximum static negative m_{xy} (kN·m/m), (l) Maximum total negative m_{xy} (kN·m/m)

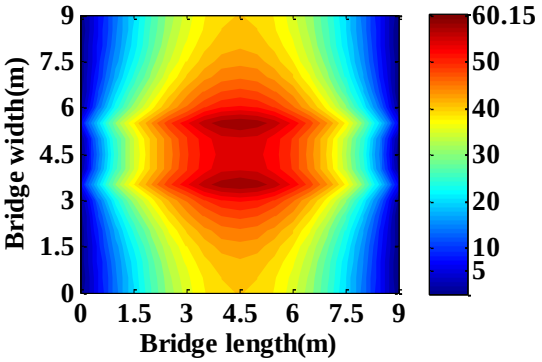
Bridge width(m)
Bridge length(m)
0 1.5 3 4.5 6 7.5 9
60.15 50 40 30 20 10 5

(a)

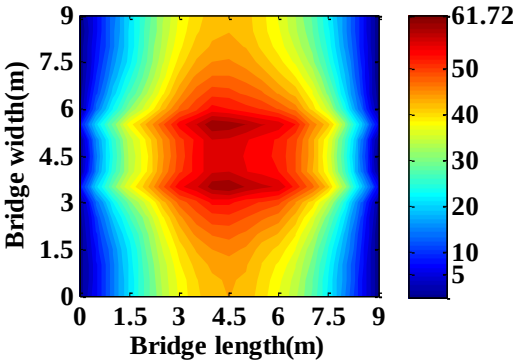
Bridge width(m)
Bridge length(m)
0 1.5 3 4.5 6 7.5 9
61.72 50 40 30 20 10 5

(b)

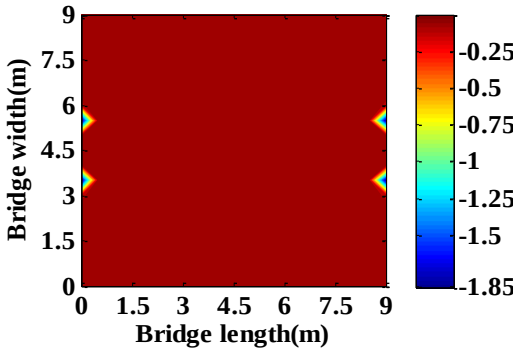
Bridge width(m)
Bridge length(m)
0 1.5 3 4.5 6 7.5 9
-0.25 -0.5 -0.75 -1 -1.25 -1.5 -1.85

(c)

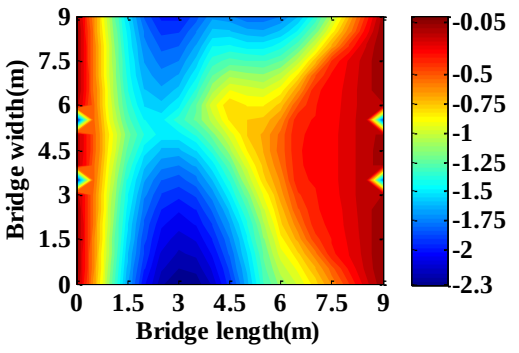
Bridge width(m)
Bridge length(m)
0 1.5 3 4.5 6 7.5 9
-0.05 -0.5 -0.75 -1 -1.25 -1.5 -1.75 -2 -2.3

(d)

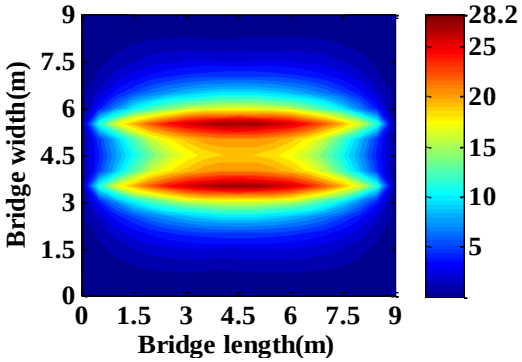
Bridge width(m)
Bridge length(m)
0 1.5 3 4.5 6 7.5 9
28.2 25 20 15 10 5

(e)

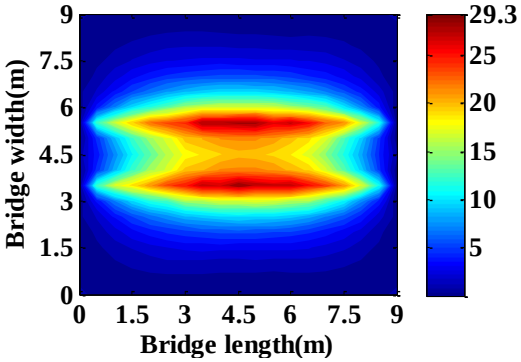
Bridge width(m)
Bridge length(m)
0 1.5 3 4.5 6 7.5 9
29.3 25 20 15 10 5

(f)

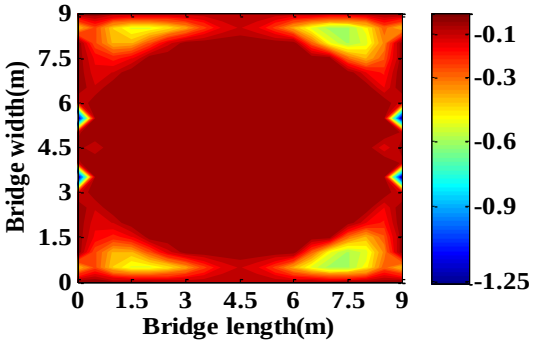
Bridge width(m)
Bridge length(m)
0 1.5 3 4.5 6 7.5 9
-0.1 -0.3 -0.6 -0.9 -1.25

(g)

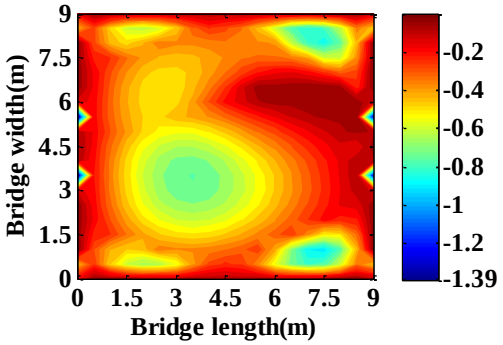
Bridge width(m)
Bridge length(m)
0 1.5 3 4.5 6 7.5 9
-0.2 -0.4 -0.6 -0.8 -1 -1.2 -1.39

(h)

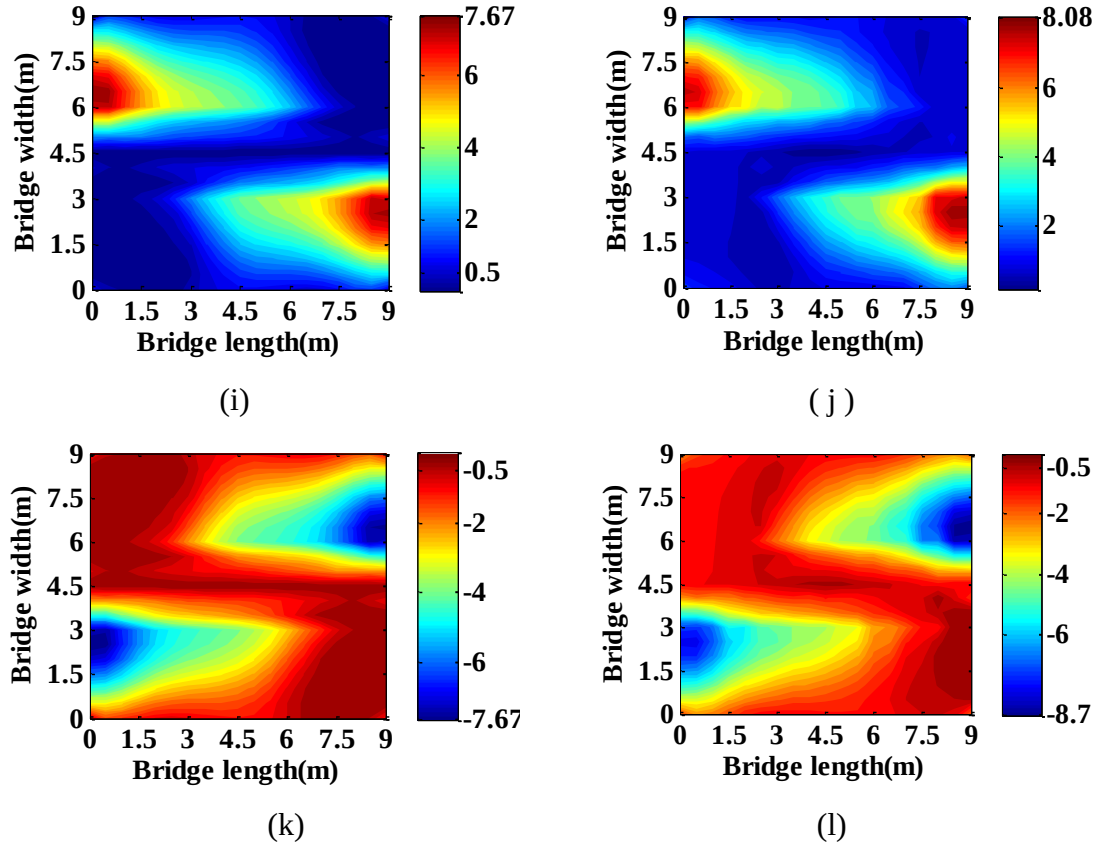

Figure 7. Envelope of maximum positive and negative moments for vehicle travelling on path '2' of the bridge at 20 m/s: (a) Maximum static positive m_x (kN·m/m), (b) Maximum total positive m_x (kN·m/m), (c) Maximum static negative m_x (kN·m/m), (d) Maximum total negative m_x (kN·m/m), (e) Maximum static positive m_y (kN·m/m), (f) Maximum total positive m_y (kN·m/m), (g) Maximum static negative m_y (kN·m/m), (h) Maximum total negative m_y (kN·m/m), (i) Maximum static positive m_{xy} (kN·m/m), (j) Maximum total positive m_{xy} (kN·m/m), (k) Maximum static negative m_{xy} (kN·m/m), (l) Maximum total negative m_{xy} (kN·m/m)

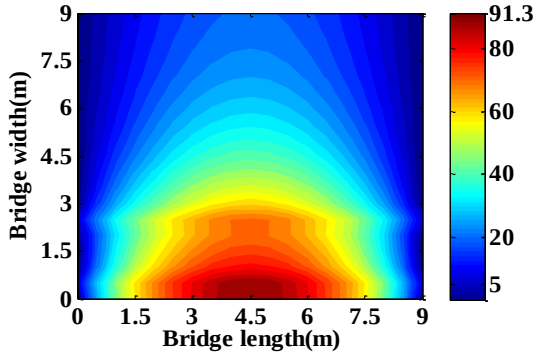
Bridge width(m)
Bridge length(m)
0 1.5 3 4.5 6 7.5 9
91.3 80 60 40 20 5

(a)

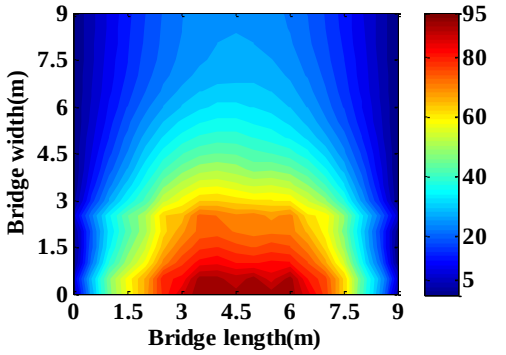
Bridge width(m)
Bridge length(m)
0 1.5 3 4.5 6 7.5 9
95 80 60 40 20 5

(b)

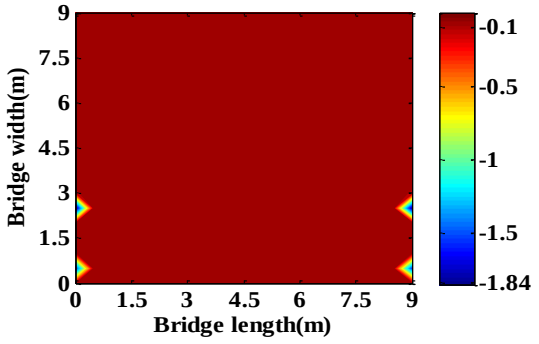
Bridge width(m)
Bridge length(m)
0 1.5 3 4.5 6 7.5 9
-0.1 -0.5 -1 -1.5 -1.84

(c)

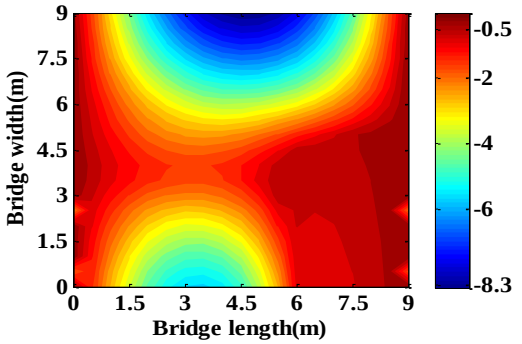
Bridge width(m)
Bridge length(m)
0 1.5 3 4.5 6 7.5 9
-0.5 -2 -4 -6 -8.3

(d)

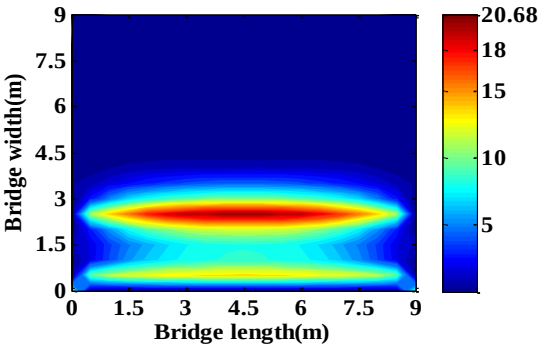
Bridge width(m)
Bridge length(m)
0 1.5 3 4.5 6 7.5 9
20.68 18 15 10 5

(e)

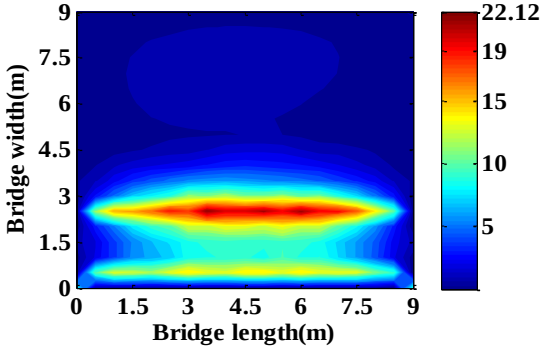
Bridge width(m)
Bridge length(m)
0 1.5 3 4.5 6 7.5 9
22.12 19 15 10 5

(f)

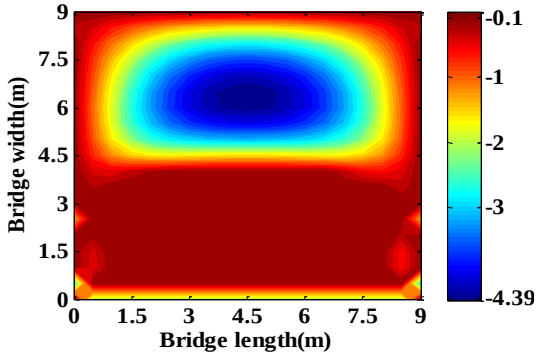
Bridge width(m)
Bridge length(m)
0 1.5 3 4.5 6 7.5 9
-0.1 -1 -2 -3 -4.39

(g)

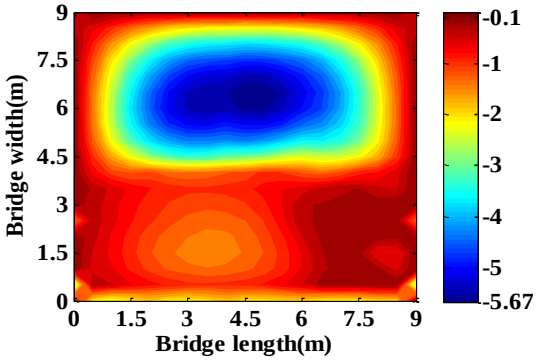
Bridge width(m)
Bridge length(m)
0 1.5 3 4.5 6 7.5 9
-0.1 -1 -2 -3 -4 -5 -5.67

(h)

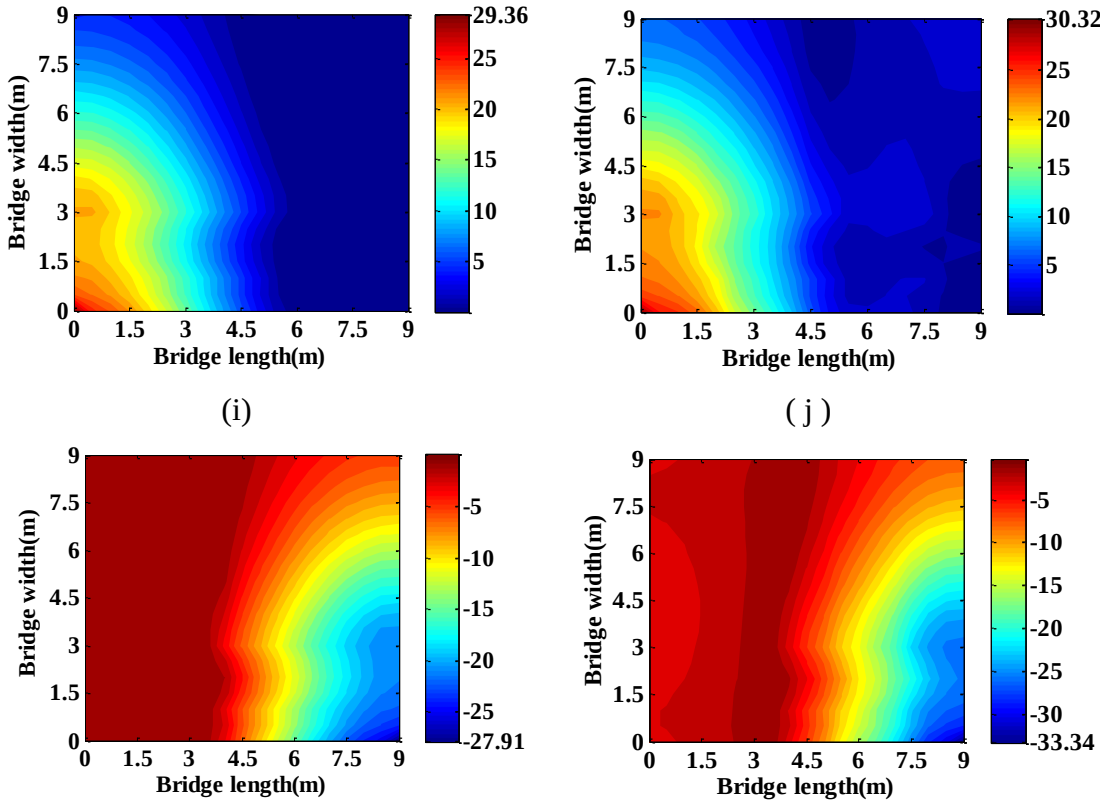

Figure 8. Envelope of maximum positive and negative moments for vehicle travelling on path '3' of the bridge at 20 m/s: (a) Maximum static positive m_x (kN·m/m), (b) Maximum total positive m_x (kN·m/m), (c) Maximum static negative m_x (kN·m/m), (d) Maximum total negative m_x (kN·m/m), (e) Maximum static positive m_y (kN·m/m), (f) Maximum total positive m_y (kN·m/m), (g) Maximum static negative m_y (kN·m/m), (h) Maximum total negative m_y (kN·m/m), (i) Maximum static positive m_{xy} (kN·m/m), (j) Maximum total positive m_{xy} (kN·m/m), (k) Maximum static negative m_{xy} (kN·m/m), (l) Maximum total negative m_{xy} (kN·m/m)

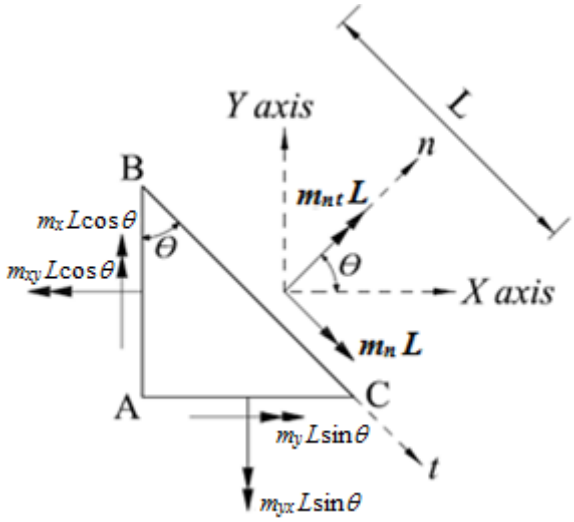

Figure 9. Plan view of moments acting on a plate slice

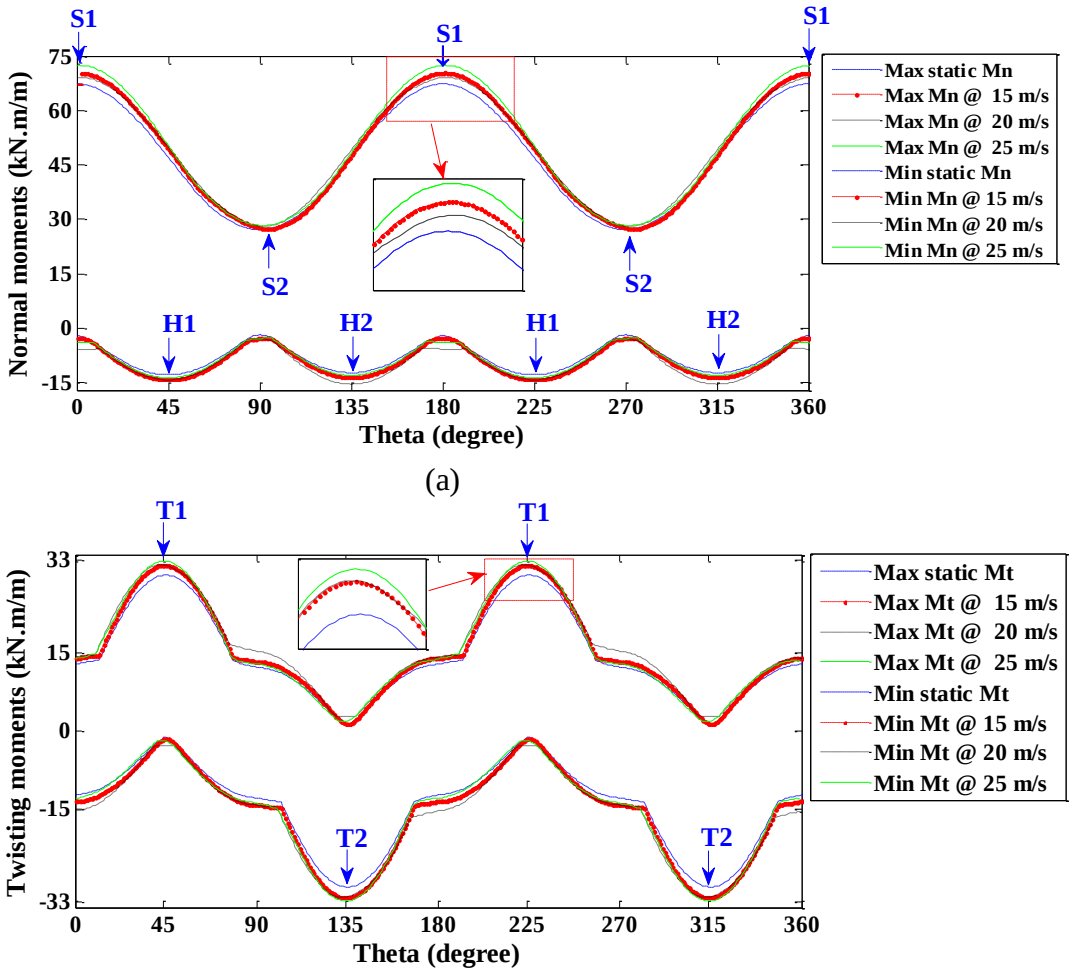

Figure 10. Static and total moments for vehicle travelling at 15, 20 and 25 m/s on path '1' of the bridge: (a) Min_m_n and Max_m_n versus θ, (b) Max_m_{nt} and Min_m_{nt} versus θ

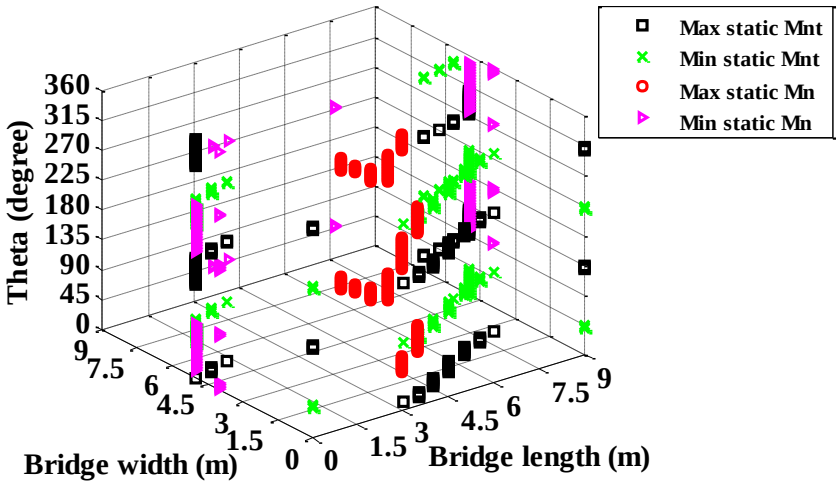

Figure 11. 3-D plot of critical locations of static moments (Max_m_n , Min_m_n, Max_m_{nt} and $Min\_m_{nt)}$ for each angle θ when vehicle travels on path '1'

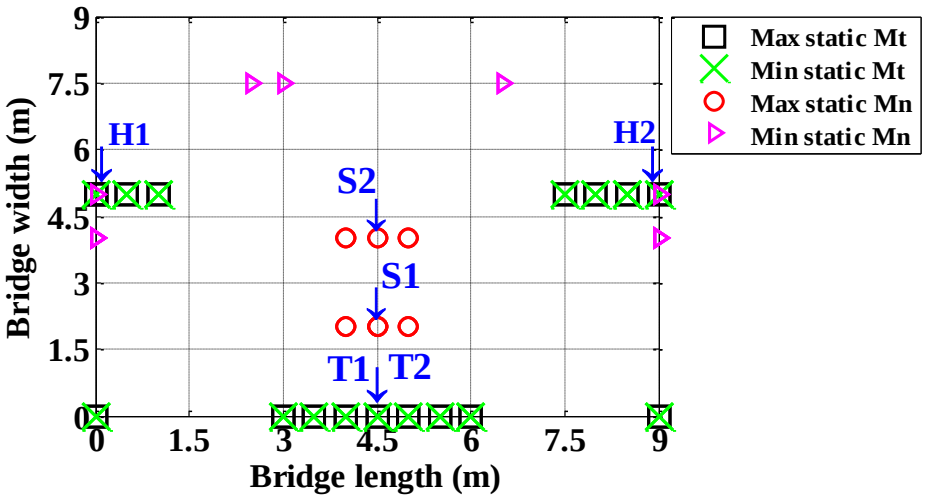
Max static Mt
Min static Mt
Max static Mn
Min static Mn
H1
H2
S2
S1
T1
T2
Bridge width (m)
Bridge length (m)
0
1.5
3
4.5
6
7.5
9

(a)

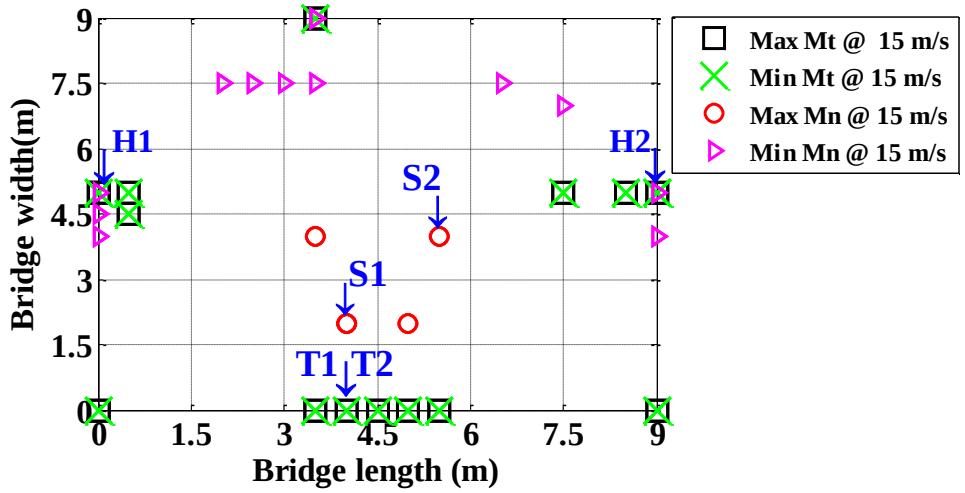
Max Mt @ 15 m/s
Min Mt @ 15 m/s
Max Mn @ 15 m/s
Min Mn @ 15 m/s
H1
H2
S2
S1
T1
T2
Bridge width(m)
Bridge length (m)
0
1.5
3
4.5
6
7.5
9

(b)

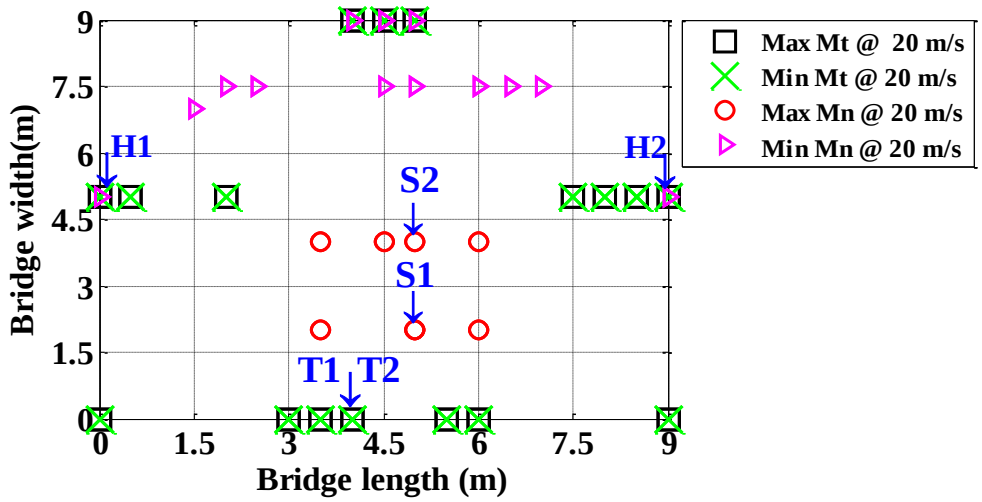
Max Mt @ 20 m/s
Min Mt @ 20 m/s
Max Mn @ 20 m/s
Min Mn @ 20 m/s
H1
H2
S2
S1
T1
T2
Bridge width(m)
Bridge length (m)
0
1.5
3
4.5
6
7.5
9

(c)

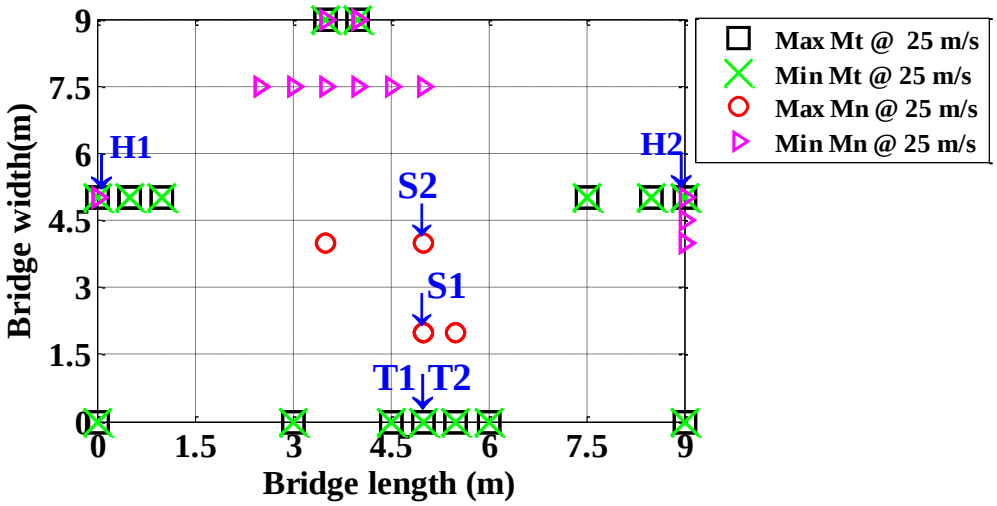

(d)

Figure 12. Critical locations of *Max_m*$_n$, *Min_m*$_n$, *Max_m*$_{nt}$ and *Min_m*$_{nt}$ for vehicle travelling on path '1': (a) Static, (b) Total at 15 m/s, (c) Total at 20 m/s, (d) Total at 25 m/s

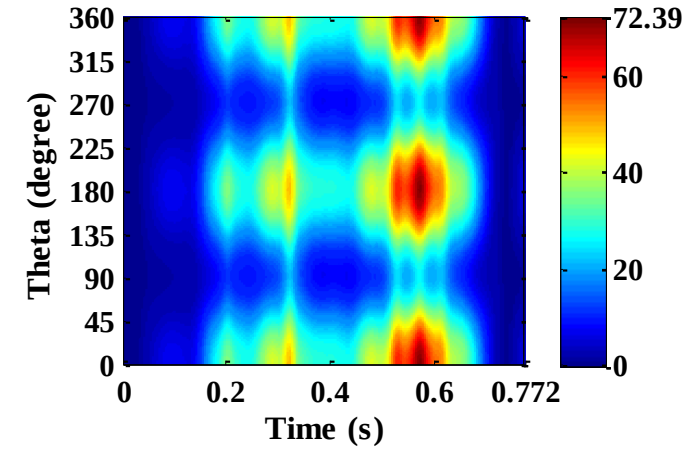

(a)

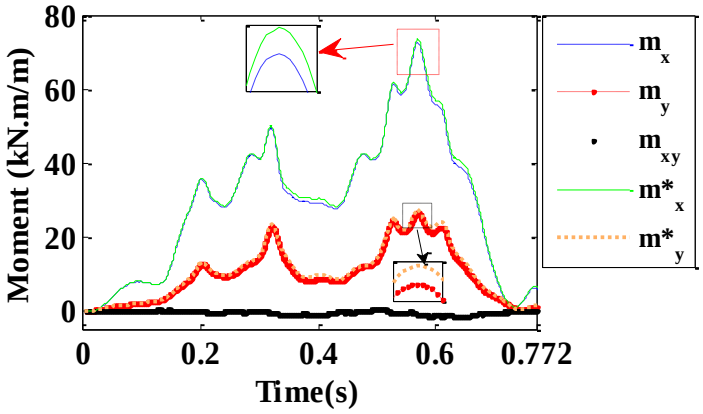

(b)

Figure 13. Moments acting on point of coordinates (X = 5 m,Y = 2 m) due to the vehicle travelling along path '1' at 25 m/s: (a) Bending moment m_n versus time and plane orientation (0 to 360 degrees), (b) m_x, m_y, m_{xy}, m_x* and m_y* versus time